Response to Review #1

Summary: Yin et al. have found a high correlation (0.51) between the early winter haze days in the North China plain and the September-October sea ice in the west of the Beaufort Sea. Further analysis revealed that the sea surface temperature anomalies over the Bering Sea and Gulf of Alaska acting as a bridge that linked the variations of haze days and sea ice. This is interesting, also important for us to understand the causing of the changes of haze pollutions over China in recent years. I recommend it to be accepted by ACP after several corrections.

1. **In recent years, there are increasing works referring to the impact of climate change on the haze pollution over China. The authors should present updating review on these new papers in the introduction.**

Reply:

The impact of climate change on haze pollution in China was a meaningful scientific issue and were paid attentions in recent years. Some related publications were cited now to update the introduction.

Revision:

…For the long-term trend of number of haze days, human activities are the recognized and fundamental driver (Li et al., 2018; Yang et al 2016; Chen et al., 2018; Zhang et al., 2018)…

…By the sensitive experiments, Li et al. (2017) emphasized the impacts of ASI anomalies on haze pollution in North China, but deemphasized the role of ENSO (He et al., 2019)…

Supplemented new papers:

Chen, H. P., Wang, H. J., Sun, J. Q., Xu, Y. Y., and Yin, Z. C.: Anthropogenic Fine Particulate Matter Pollution Will Be Exacerbated in Eastern China Due to 21st-Century GHG Warming, Atmos. Chem. Phys. Discuss., https://doi.org/10.5194/acp-2018-761, in review, 2018.

He, C., Liu, R., Wang, X. M., Liu, S. C., Zhou, T. J., Liao, W. H.: How does El Niño-Southern Oscillation modulate the interannual variability of winter haze days over eastern China? Science of the Total Environment, 651, 1892–1902, https://doi.org/10.1016/j.scitotenv.2018.

10.100, 2019.

Zhang, Q. Q., Ma, Q., Zhao, B., et al.: Winter haze over North China Plain from 2009 to 2016: Influence of emission and meteorology, Environmental Pollution, 242: 1308–1318, 2018.

2. **Line 46: The reference here is not found in the reference list. "2017" may be "2016"?**

Reply:

The error was revised.

Revision:

…but the rapid ASI decline also contributed to the trend of number of haze days in the North China Plain after 2000 (Wang and Chen 2016)…

3. **Some information for the site observation should be clear. For example, how many meteorological sites used here? as well as the number of monitoring sites for PM2.5. How to deal with the missing values.**

Reply:

(1) The sites used here was shown in Figure 1. The cross (dot) indicated that the HDJ accounted for more (less) than 70% of the total winter haze days.

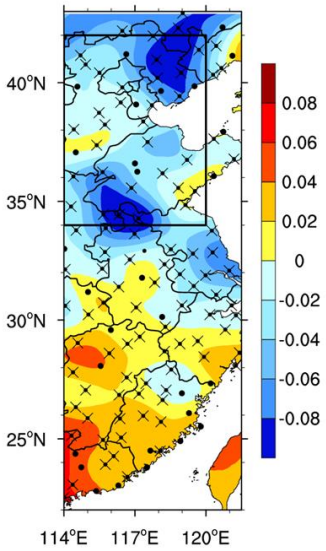

(2) More information were added. The number of meteorological sites were used to calculated the HDJ_{NCP} was 38, and the number of $PM_{2.5}$ sites were 162.

(3) The sites with missing values >5% was discarded, the others were kept in the datasets.

Revision:

In this study, we focused on the HDJ in the NCP region (HDJ_{NCP}, i.e., mean of the 38 sited HDJ) and its connection with the autumn ASI.

The hourly $PM_{2.5}$ concentration data were provided by the Ministry of Environmental Protection of China, including 162 sites in the North China.

4. The definition of the haze pollution should be clear.

Reply:

The definition of haze was added in the manuscripts.

Revision:

That is, if the visibility was lower than 10km and the relative humidity was drier than 90%, the day was defined as one haze day after filtering the other weather affected visibility (i.e., precipitation, dust, sandstorm, etc.).

5. Line 84-85: This expression here is not correct. Here, just the number of haze days is highlighted, not the synoptic process.

Reply:

The error was revised.

Revision:

The daily maximum of area-mean $PM_{2.5}$ in 2015 is shown in Figure 2b and was above 100 μg/m³. The ~~synoptic processes of haze~~ concentrations of $PM_{2.5}$ were relatively ~~weaker~~lower in January 2016 than those in December but still exceeded the threshold of pollution in China (i.e., 75 μg/m³). On 23 December, the most disastrous haze occurred, and the area-mean

6. Line 90-92: The linear trend here has been deleted or not? It should be clear here as well as in the figure caption.

Reply:

To emphasize the interannual variation, the linear trend was removed.

Revision:

…the correlation coefficients between the HDJ_{NCP} and the September-October sea ice were assessed after removing the linear trend (Figure 3)…

7. Line 105: the "heavy" used here is not correct, as well as in the other places throughout MS.

Reply:

The error was revised throughout the MS.

Revision:

The ~~heavy~~ positive sea ice anomalies, with high albedo, can efficiently reflect solar radiation and restore more fresh water, which could influence the local and adjacent SST. The correlation coefficients between BSISO and the simultaneous and subsequent SST were computed (Figure 5). Because of efficient reflections of the solar radiation, the locally negative SST anomalies, located near the west of the Beaufort Sea (70–81°N, 166°E–138°W), were ~~induced by~~associated with the ~~heavy~~ positive BSISO anomalies in October. In the following two months, these negative SST anomalies could not be sustained, i.e., these anomalous responses disappeared in November. However, the ~~induced~~ positive SST anomalies in the

8. As we all know, the wind is one of key factor that exerts impact on the haze pollution. Compared to the zonal wind, the meridional wind generally performs a greater role on the particulate dissipation. So, the influence of the sea ice on the meridional wind should be checked.

Reply:

The arrows in Figure 14a was the influences of the SST_{BA} on the surface wind and has included the meridional wind.

Furthermore, we also plotted the required Figures, but did not repeat it in the manuscript. The SST_{BA} was the bridge to connect the number of haze days and the sea ice anomalies. In the flowing Figure, the surface meridional wind showed significantly positive correlation with the SST_{BA}. The positive correlation indicate enhanced southerly anomalies, which weakened the cold air from the high latitude and make the dissipation conditions poor. Thus, the haze occurred easily.

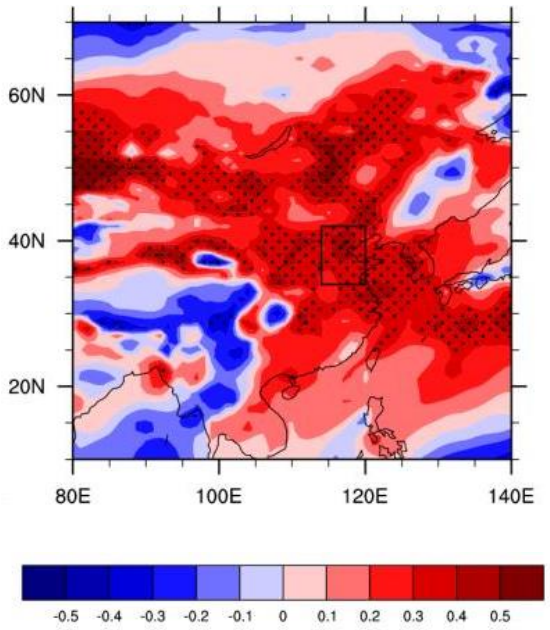

Figure. The CC between the November SST_{BA} and surface meridional wind, the black dots indicate that the CC exceeded the 95% confidence level

Revision:

cold air and ventilation conditions. Compared to the local zonal wind, the meridional wind played more important roles on weakening the horizontal dissipation conditions of the air (Figure omitted). The ~~induced~~ southerly anomalies were located over the coastal area of China and transported moisture to the NCP area (Figure 14a), providing moist air for haze formation.

9. What about the relationship between the local wind speed and Beaufort Sea ice/SST anomalies over the Bering Sea and Gulf of Alaska?

Reply:

We plotted the required Figures as follows. It is obvious that the relationship between the local wind speed and Beaufort Sea ice/SST anomalies over the Bering Sea and Gulf of Alaska was negative, but the relationship was not as significant as the meridional wind. (1) The wind speed anomalies associated with preceding sea ice/SST anomalies were negative. The smaller wind speed indicate poor horizontal dissipation conditions in the air, thus the particulates accumulated efficiently. (2) In weakening the horizontal dissipation, the changed of the meridional wind played more important roles.

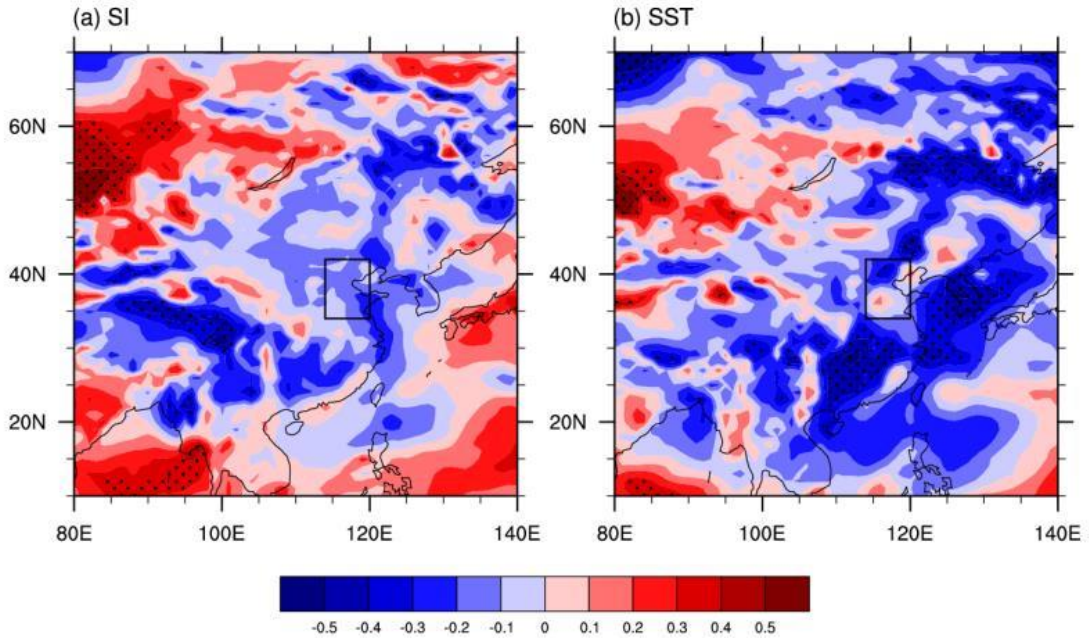

Figure. The CC between the (a) BSISO, (b) November SST_{BA} and surface meridional wind, the black dots indicate that the CC exceeded the 95% confidence level

Revision:

cold air and ventilation conditions. Compared to the local zonal wind, the meridional wind played more important roles on weakening the horizontal dissipation conditions of the air (Figure omitted). The ~~induced~~ southerly anomalies were located over the coastal area of China and transported moisture to the NCP area (Figure 14a), providing moist air for haze formation.

10. The English writing should be further improved.

Reply:

The English has been improved the native speaker.

Response to Review #2

General comments: Haze pollution is for the time being a serious problem for China. The prediction of haze pollution is highly-relevant to the society. The manuscript explored the linkage between the number of haze days in China and the change in autumn sea ice extent in the Beaufort Sea and analyze the potential mechanism. I find the manuscript is scientifically interesting and fits the scope of ACP. However, major revision is needed before it can be accepted for publication in ACP

Major comment:

1. the cause and effect are not convincing in this manuscript. There are quite some places authors used 'induced'. Correlation/regression can not tell what is cause and what is the effect.

Reply:

(1) To verify the proposed causality, numerical experiments were designed by the public CESM-LE datasets. **A new section "5. Causality verification by CESM-LE experiments" and a new Figure 16 was added in the manuscript.**

The CESM-LE simulations were completed by the fully coupled CESM model, thus the interactions among sea ice, sea temperature and atmosphere can be contained. In the numerical experiment, all available CESM-LE members were included and different amplitudes of sea ice anomalies were composited, thus the uncertainty from the internal variability were largely reduced.

In this experiment, **the linkages between the BSISO and the haze pollution in the North China also exist in CESM-LE simulations.** Meanwhile, the corresponding physical mechanisms were also well reproduced by the large ensemble members. Details can be found in the following revision.

(2) In the old version, in addition to the correlation analysis, the composite results were also included, such as Figure 4 and 16 (17 now). In Figure 4, every years with significant BSISO anomalies were analyzed to find the corresponded haze conditions. Furthermore, a typical case (i.e., 2015) was studied to confirm the

proposed relationship.

Revision:

5. Causality verification by CESM-LE experiments

The connection between the haze pollution in North China and ASI, and associated physical mechanisms were statistically analyzed. To confirm the causality, numerical experiments were designed with the public CESM-LE datasets. To be consistent with the observational results, the variables from CESM-LE from 1979 to 2015 are employed, which was combined by the historical simulation during 1979–2005 and the data during 2006–2015 from the future representative concentration pathway 8.5 (RCP8.5 scenario) forcing simulation. 35 CESM-LE ensemble members were used here. The CESM-LE simulations were completed by the fully coupled CESM model, thus the interactions among sea ice, sea temperature and atmosphere can be contained. **The years when the sea ice anomalies concentrated in the west of the Beaufort Sea were selected and the differences between the positive BSISO and negative BSISO years were be identified as the responses to the sea ice anomalies.** In the numerical experiment, all available CESM-LE members were included and different amplitudes of sea ice anomalies were composited, thus the uncertainty from the internal variability were largely reduced.

In Figure 16a, the sea ice anomalies were obvious in the key region. The maximum of the difference in sea ice concentration was more than 35% (Figure 16a). In the following November, the accumulated sea ice favored increased SST over the Gulf of Alaska (Figure 16b), which is in good accordance with the observed results. Although there were weaker, but negative SST responses in Bering Sea, the positive SST anomalies extended southwards and enhanced the air-sea interaction. In terms of the corresponding atmospheric circulations with regard to anomalous BSISO, the composite difference was also consistent with the observed results. The anti-cyclonic anomalies of the geopotential height at 500hPa were also well reproduced by the model in the early winter (Figure 16c). On the lower troposphere, there were also anomalous anticyclone over North China and Northeast China, which induced anomalous southerlies (Figure 16d) and weakened the cold air from the high latitude.

Furthermore, the moist air condition (Figure 16c) and lower boundary layer (Figure 16d) were also verified to be significantly connected with the positive BSISO anomalies. **Consistent with the observed results, the linkages between the BSISO and the haze pollution in the North China also exist in CESM-LE simulations.** Meanwhile, the corresponding physical mechanisms were also well reproduced by the large ensemble members. The performances of numerical models in the mid-high latitude were consistently limited, however, the results from CESM-LE here successfully captured major features and general physical processes as expected. Consequently, the robustness of the proposed connections and physical mechanisms were strongly confirmed.

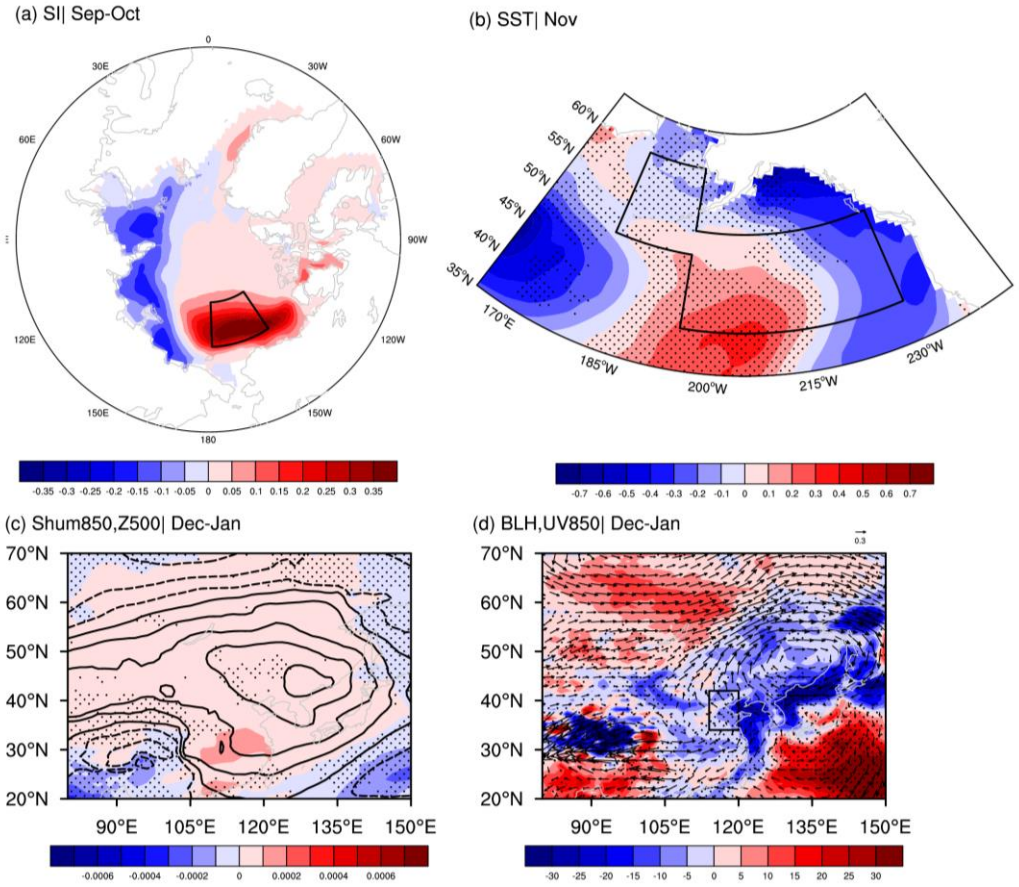

Figure R1. Composite difference of (a) September-October sea ice concentration, (b) sea surface temperature in November, (c) geopotential height (contour) at 500 hPa, specific humidity at 850 hPa in December-January, (d) BLH (shading), wind (arrow) at 850 hPa in December-January. The black box in panel (a) represents the location of the Beaufort Sea, and in panel (b) it represents the BA area. Results are based on 35 ensembles of CESM-LE simulations. The black dots indicate that mathematical sign of the changes with shading from more than 50% of the members are consistent with

the ensemble mean.

2. Why can not directly link the SST anomalies in the Bering Sea and the number of haze days over NCP?

Reply:

Certainly, there was directly link between the November SST anomalies and the number of haze days in December and January. There are two reasons why we link the number of haze days and the September-October sea ice. (1) As an efficient driver, the September-October sea ice was one month in advance of the November SST, which **supports sufficient time gap to make the seasonal prediction in the real-time operation.** That is, in November, we may gain the sea ice September-October data and run the statistical seasonal prediction models. (2) The goal of this manuscript is to reveal the connection between the sea ice and the haze pollution in the early winter. Our studies **not only reveal the link between the SST and haze, but also deepen the understanding the impacts of the sea ice on the haze** by taking the SST anomalies as a bridge.

Detailed comments:

1. What is the difference between 'Arctic region' (Line 23) and 'Arctic area' (Line 25)?

Reply:

The presentations were coalesced to "Arctic region".

Revision:

~~tremendous concerns from global climate change scientists.~~ During the past few years, the increase of surface air temperature has been distinctly amplified in the Arctic ~~area~~ region~~(i.e., the Arctic Amplification feature)~~ and approximately

2. Line 23, I do not understand why authors highlighted 'February 2018' since no data from 2018 is used in the manuscript.

Reply:

In the old version, we mentioned 'February 2018' to emphasize the importance of

Arctic sea ice. Now, to focus on the scientific issue, the associated texts were deleted.

Revision:

~~In February 2018, the highest temperature near the Arctic region was above the freezing point (Jason, 2018), raising tremendous concerns from global climate change scientists.~~ During the past few years, the increase of surface air temperature has been distinctly amplified in the Arctic ~~area~~ region~~(i.e., the Arctic Amplification feature)~~ and approximately

3. Line 24, Does the authors mean the Arctic amplification intensified only during past few years?

Reply:

Our presentation was confusing. We did not mean the Arctic amplification intensified. We wanted to introduce that the increase of surface air temperature has been distinctly amplified in the Arctic region and lead to the definition of Arctic amplification.

The confusing texts have been revised.

Revision:

~~tremendous concerns from global climate change scientists.~~ During the past few years, the increase of surface air temperature has been distinctly amplified in the Arctic ~~area~~ region~~(i.e., the Arctic Amplification feature)~~ and approximately twice as large as the average increase in global warming, which was called the Arctic Amplification (Zhou, 2017). ~~Recently,~~

4. Line 26, What the authors mean by 'Recently'?

5. Line 26, 'Arctic sea ice decreases rapidly since the satellite era, in particular, after year 2000'.

Reply:

According to the advice of the reviewer, detailed comments 4 &5 were revised together.

Revision:

…Arctic sea ice (ASI) decreases rapidly since the satellite era, in particular, after the year of 2000 (Gao et al., 2015)…

twice as large as the average increase in global warming, which was called the Arctic Amplification (Zhou, 2017). ~~Recently, the~~ Arctic sea ice (ASI) decrease~~sd rapidly due to the Arctic Amplification and reached a record low in September 2012~~since the satellite era, in particular, after the year of 2000 (Gao et al., 2015). The ~~loss~~ change of ASI, associated with changed the

6. Line 27, 'the change of ASI'

Reply:

According to the advice of the reviewer, the errors were revised.

Revision:

…The change of ASI, associated with changed reflection of solar radiation and the exchange of energy and fresh water, could remotely connect with the climate in the Northern Hemisphere, especially the winter climate in Eurasia…

7. Line 30, remove 'variability'

Reply:

According to the advice of the reviewer, the errors were revised.

Revision:

…especially the winter climate in Eurasia…

8. Line30, sea ice is a component in climate system, is not an external driver

Reply:

According to the advice of the reviewer, the errors were revised.

Revision:

climate in the Northern Hemisphere, especially the winter climate ~~variability~~ in Eurasia (Liu et al., 2007; Wang and Liu, 2016). ~~As an efficient external driver in the high latitudes, t~~The decreased ASI over the Barents–Kara Seas in late autumn stimulated a planetary-scale Rossby wave train in early winter (Honda et al., 2009; Kim et al., 2014) and transported its

9. Line 40, it is better if the authors can provide a brief definitions for dust,

sandstorm and haze.

Reply:

The brief definitions for dust, sandstorm and haze were provided.

Revision:

…The dust (dry particles suspended in air after strong wind) and sandstorm (strong wind carrying sand) over North China, types of weather that are sensitive to wind, also showed close relationships with the variation of ASI after the mid-1990s (Fan et al., 2017)…

…Haze (polluted particulate aerosols suspended in air), also being sensitive to wind, frequently occurred under calm and static weather conditions…

10. Line 45, 'long-term trend of haze' is not clear. Long-term trend of number of haze days, or intensity of haze, or periods of haze?

11. Line 46, the same as above 'the trend of haze pollution'

12. Line 50, the same as above, 'correlation with the haze'

13. Line51, the same as above, 'different variations in haze days'

14. Line 52, 'between the autumn sea ice cover in Beaufort Sea and the number of haze days in winter'

15. Line54. 'number of haze days varied differently during early (December-January) and late (February) winters'

Reply:

The presentation "haze days" was confusing and should be **the number of the haze days**. Detailed comments 10–15 were revised together.

Revision:

Haze (polluted particulate aerosols suspended in air), also being sensitive to wind, frequently occurred under calm and static weather conditions, i.e., small surface winds and strong thermal inversion (Yin et al., 2015; Ding and Liu, 2014; Chen and Wang, 2015; Cai et al., 2017; Gao and Chen, 2017). For the long-term trend of number of haze days, human activities are the recognized and fundamental driver (Li et al., 2018; Yang et al 2016; Chen et al., 2018; Zhang et al., 2018), but the rapid ASI decline also contributed to the trend of number of haze days~~haze pollution~~ in the North China Plain after 2000 (Wang and Chen 2016~~7~~). For the interannual to interdecadal variations, the impacts of ASI on the number of haze days~~haze~~ in the east of China were emphasized by observational analyses (Wang et al., 2015) and numerical studies (Li et al. 2017). By the sensitive experiments, Li et al. (2017) emphasized the impacts of ASI anomalies on haze pollution in North China, but deemphasized the role of ENSO (He et al., 2019). From 1979–2012, the ASI loss led to a northward shift of the East Asia jet stream and weak East Asian winter monsoons, indicating a strongly negative correlation with the number of haze days~~haze~~ in the east of China (Wang et al. 2015). However, the first mode of the Empirical Orthogonal Function (EOF) in Yin and Wang (2016a) presented different variations of number of haze days~~haze days~~ in the south and north of the Yangtze River. The positive relationship between the autumn sea ice in the Beaufort Sea and the number of haze days in winter ~~haze days~~ was briefly revealed without sufficient physical explanations but contributed to the prediction of number of haze days in winter ~~haze days~~ (Yin and Wang 2016b, 2017b). The number of haze days in early winter (December-January) ~~haze days~~ also varied differently with that in~~e~~ February ~~haze days~~ (figure omitted), ~~indicating a variant modulating mechanism from~~

16. Line 54', 'suggesting a potential different driving mechanism'

Reply:

According to the advice of the reviewer, the errors were revised.

Revision:

…The number of haze days in early winter (December-January) also varied differently with that in February (figure omitted), suggesting a potential different driving mechanism…

17. Line 56, similar as No. 14

Reply:

The presentation "haze days" was confusing and should be the number of the haze days.

Revision:

…Thus, an open question still existed, i.e., the connections between Beaufort Sea ice (BSI) and the number of haze days in early winter in the North China Plain (NCP: 34–42^{o}N, 114-120^{o}E) and the associated physical mechanisms…

18. Line 80', 'The HDJ was stable during 1979 to 2012 and decreased during 1993 to 2009'

Reply:

According to the advice of the reviewer, the confusing presentation were revised.

Revision:

…The HDJ_{NCP} was stable during 1979 to 1992 and decreased from 1993 to 2009…

19. Line 80, 'The HDJ showed a strong upward trend after 2009'

Reply:

According to the advice of the reviewer, the confusing presentation were revised.

Revision:

…After 2009, the HDJ_{NCP} showed a strong upward trend…

20. Line 85, 'what is the threshold for pollution in China'?

Reply:

The threshold was supplemented.

Revision:

…still exceeded the threshold of pollution in China (i.e., 75 μg/m^{3})…

21. Line 84, what is the meaning of 'synoptic process of haze were weaker'? How to judge this?

Reply:

The "synoptic processes of haze" was not accurate. According to the advice of the reviewer, the confusing presentation were revised.

"synoptic processes of haze"→"the concentrations of $PM_{2.5}$"

Revision:

The daily maximum of area-mean $PM_{2.5}$ in 2015 is shown in Figure 2b and was above 100 μg/m³. The ~~synoptic processes of haze~~ concentrations of $PM_{2.5}$ were relatively ~~weaker~~lower in January 2016 than those in December but still exceeded the threshold of pollution in China (i.e., 75 μg/m³). On 23 December, the most disastrous haze occurred, and the area-mean

22. Line 90, there are number of places the authors used haze days. I believe that authors mean 'number of haze days'.

Reply:

The haze days were revised to the "number of haze days" throughout the MS.

Revision:

of China by modulating the large-scale atmospheric circulations and local meteorological conditions. Furthermore, the opposite pattern of number of haze days~~haze days~~ in the east of China was revealed in Figure 1. To confirm the response of

23. Line 97, the correlation cannot tell which causes which.

24. Line 101, 'correspond' instead of 'induce'. Again, correlation cannot tell which causes which

26. Line 103, 'response' is not accurate here

27. Line 108, SST and sea ice concentration in general co-varies. Correlation can not tell which causes which. Authors can also check the surface heat flux.

28. Line 108, 'induced' is not correct here.

30. Line 110, correlation can not tell 'change of BS sea ice' can lead to SST anomalies over the BS and GA. 'induced' is not correct here.

32. Line 123, how authors can conclude the change in atmosphere circulation is a response to change in sea ice by correlation?

33. Line 125, 'induced' again

34. After line 125, authrs used correlation to conclude the sea ice change-leading to atmosphere change-leading to SST change in number of places of the manuscript.

Reply:

Detailed comments 23, 24, 26–28, 30, 32–34 concentrated on the meaning of the correlation method and were similar with the Major comment 1.

(1) During the statistical analysis sections, the presentations, like “induce”, “response”, were modified.

(2) To verify the proposed causality, numerical experiments were designed by the public CESM-LE datasets. **A new section “5. Causality verification by CESM-LE experiments” and a new Figure 16 was added.**

(3) Analysis about the surface heat flux was done in Figure 9. As follows:

…the reduction of $WSPD_{RS1}$ resulted in a warmer sea surface over the Gulf of Alaska (Figure 9a). Due to the weakening of the water evaporation, the latent heat release slowed down both in the Bering Sea and the Gulf of Alaska, which conserved more thermal energy in the sea surface (Figure 9b). In addition, the upper anti-cyclonic circulations, with clear sky, facilitated more shortwave solar radiation onto the sea surface. The absorbed and stored thermal energy, which was connected with the heavy positive BSISO anomalies, heated the sea surface over the Gulf of Alaska in November, i.e., positive SST_{GA} anomalies.

Revision:

(1) 5. Causality verification by CESM-LE experiments

The connection between the haze pollution in North China and ASI, and associated physical mechanisms were statistically analyzed. To confirm the causality, numerical experiments were designed with the public CESM-LE datasets. To be consistent with the observational results, the variables from CESM-LE from 1979 to 2015 are employed, which was combined by the historical simulation during 1979–2005 and the data during 2006–2015 from the future representative concentration pathway 8.5 (RCP8.5 scenario) forcing simulation. 35 CESM-LE ensemble members were used here. The CESM-LE simulations were completed by the fully coupled

CESM model, thus the interactions among sea ice, sea temperature and atmosphere can be contained. **The years when the sea ice anomalies concentrated in the west of the Beaufort Sea were selected and the differences between the positive BSISO and negative BSISO years were be identified as the responses to the sea ice anomalies.** In the numerical experiment, all available CESM-LE members were included and different amplitudes of sea ice anomalies were composited, thus the uncertainty from the internal variability were largely reduced.

In Figure 16a, the sea ice anomalies were obvious in the key region. The maximum of the difference in sea ice concentration was more than 35% (Figure 16a). In the following November, the accumulated sea ice favored increased SST over the Gulf of Alaska (Figure 16b), which is in good accordance with the observed results. Although there were weaker, but negative SST responses in Bering Sea, the positive SST anomalies extended southwards and enhanced the air-sea interaction. In terms of the corresponding atmospheric circulations with regard to anomalous BSISO, the composite difference was also consistent with the observed results. The anti-cyclonic anomalies of the geopotential height at 500hPa were also well reproduced by the model in the early winter (Figure 16c). On the lower troposphere, there were also anomalous anticyclone over North China and Northeast China, which induced anomalous southerlies (Figure 16d) and weakened the cold air from the high latitude. Furthermore, the moist air condition (Figure 16c) and lower boundary layer (Figure 16d) were also verified to be significantly connected with the positive BSISO anomalies. **Consistent with the observed results, the linkages between the BSISO and the haze pollution in the North China also exist in CESM-LE simulations.** Meanwhile, the corresponding physical mechanisms were also well reproduced by the large ensemble members. The performances of numerical models in the mid-high latitude were consistently limited, however, the results from CESM-LE here successfully captured major features and general physical processes as expected. Consequently, the robustness of the proposed connections and physical mechanisms were strongly confirmed.

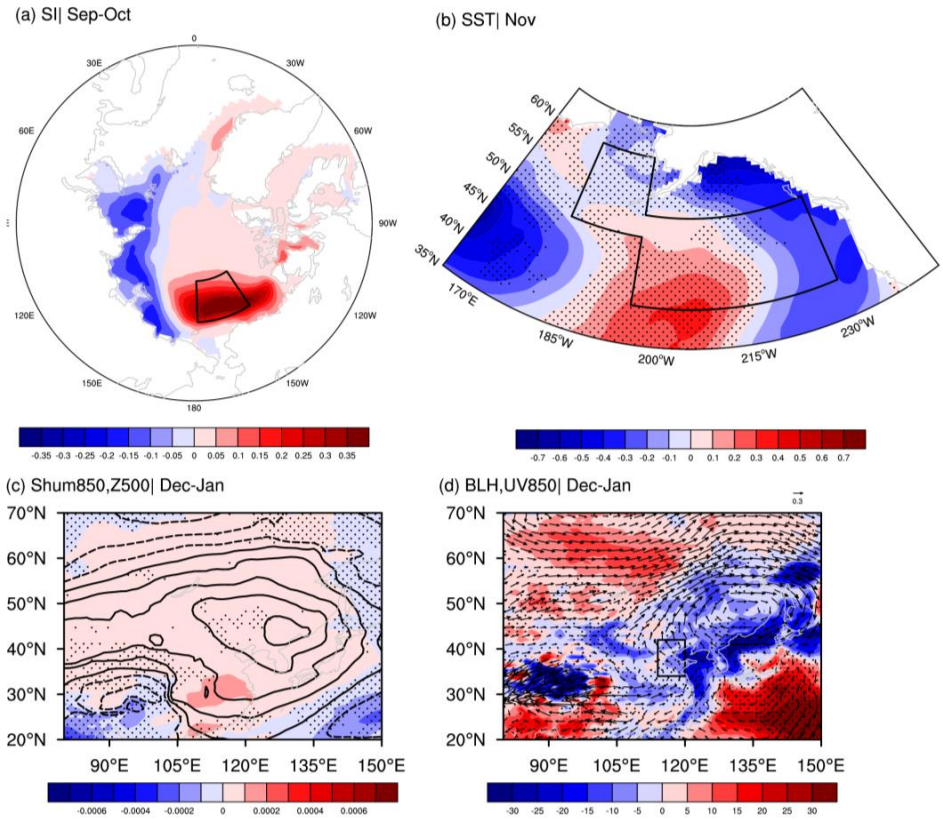

Figure R1. Composite difference of (a) September-October sea ice concentration, (b) sea surface temperature in November, (c) geopotential height (contour) at 500 hPa, specific humidity at 850 hPa in December-January, (d) BLH (shading), wind (arrow) at 850 hPa in December-January. The black box in panel (a) represents the location of the Beaufort Sea, and in panel (b) it represents the BA area. Results are based on 35 ensembles of CESM-LE simulations. The black dots indicate that mathematical sign of the changes with shading from more than 50% of the members are consistent with the ensemble mean.

(2)

deviation). During 65% of these years, the significant BSISO anomalies corresponded ~~induced~~ HDJ_{NCP} anomalies with the same mathematical sign. There were no significantly opposite responses of HDJ_{NCP} ($|HDJ_{NCP}| > 0.8\times$its standard deviation) to the BSISO anomalies. Furthermore, the relationship seemed to be enhanced after the mid-1990s. The same mathematical signs of the anomalies appeared more frequently~~., and the intensity of the responses was also amplified.~~

The ~~heavy~~ positive sea ice anomalies, with high albedo, can efficiently reflect solar radiation and restore more fresh water, which could influence the local and adjacent SST. The correlation coefficients between BSISO and the simultaneous and subsequent SST were computed (Figure 5). Because of efficient reflections of the solar radiation, the locally negative SST anomalies, located near the west of the Beaufort Sea (70–81°N, 166°E–138°W), were ~~induced by~~associated with the ~~heavy~~ positive BSISO anomalies in October. In the following two months, these negative SST anomalies could not be sustained, i.e., these anomalous responses disappeared in November. However, the ~~induced~~ positive SST anomalies in the Bering Sea (49–60 °N, 165°W–180°W) and the Gulf of Alaska (40–52°N, 130°W–165°W) appeared in October and were

25. Line 102, can authors perform sliding correlation to indicate the enhanced connection after mid-1990?

Reply:

The sliding (21-yr running) correlation was plotted in Figure R2. It is obvious that the correlation coefficient was insignificant before 2000, but became significant then. The correlation coefficient during 1980–1997 was 0.11, but was 0.55 during 1998–2015. Furthermore, the number of years when the anomalies of HDJ_{NCP} and BSISO with the same mathematical sign (NY_{SMS}) were counted and those with significant amplitudes (i.e., |anomalies| > 0.8 × its standard deviation) among the NY_{SMS} values were extracted and termed NY_{SA}. Compared to P1, both NY_{SMS} and NY_{SA} significantly increased during P2. Specifically, there were 8 (0) NY_{SMS} (NY_{SA}) years before the mid-1990s, which dramatically increased to 13 (5) years during 1998–2015 (Figure R3).

To answer the reasons for the change of the correlationship, a paper titled "Enhanced Contributions of Beaufort Sea Ice to Early-winter Haze Days in North China after the mid-1990s" was prepared.

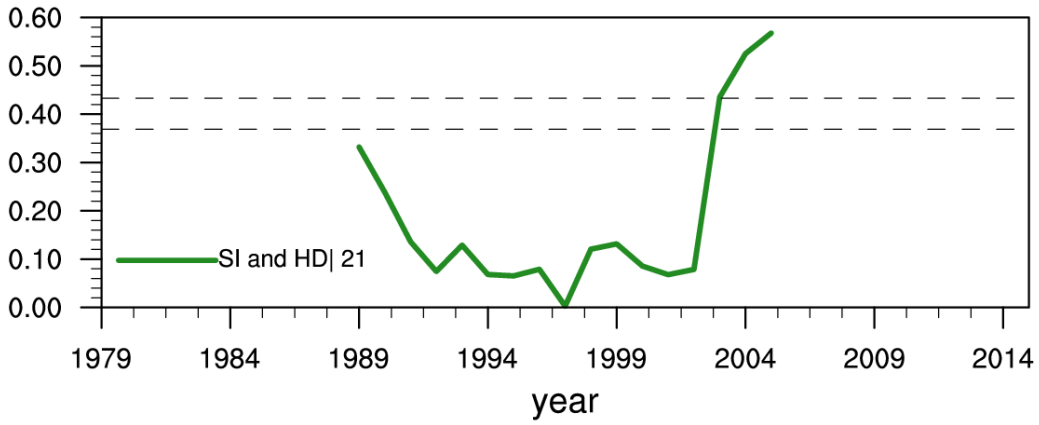

Figure R2. The 21-yr running correlation coefficient between BSISO and HDJ_{NCP}

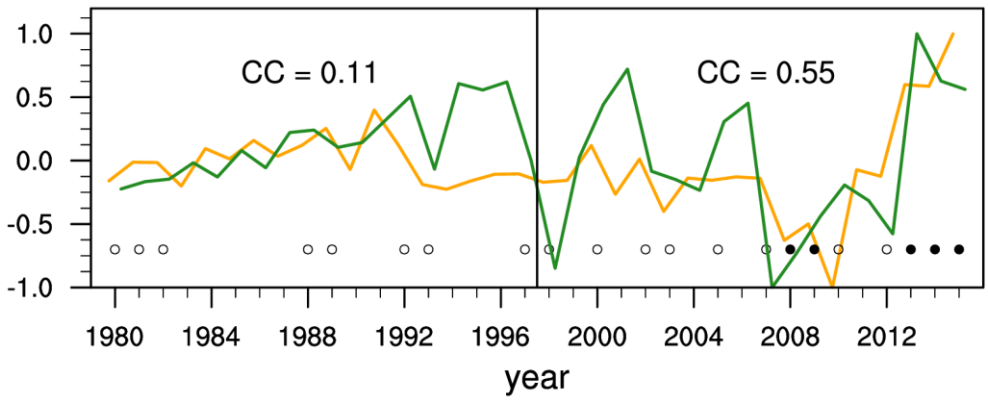

Figure R3. The variation in normalized HDJ_{NCP} (orange) and BSISO (green) from 1980 to 2015 after the removal of the linear trend. The "○" indicates the anomalies of HDJ_{NCP} and BSISO with the same mathematical sign. The "●" indicates the anomalies of HDJ_{NCP} and BSISO with significant amplitudes (i.e., |anomalies| > 0.8 × its standard deviation).

29. Line 109, Do authors have any idea why negative SST anomalies disappear in November?

Reply:

This question was not the mainly concerned issue of this manuscript, but we tried to provide a reasonable guess.

The disappearing of the negative SST anomalies in November connected with the change of the atmospheric circulations and can be explained by Figure 6 in the manuscript. (1) The September-October negative SST anomalies in the west of Beaufort Sea co-varied with the positive sea ice anomalies. (2) According to many previous studies, the signal of the ice in the polar region cannot persistent for long time by itself. **Its influence should delivery via the change of the atmospheric circulations.** (3) In Figure R4 (i.e., Figure 6 in the MS), the distribution and intensity of the atmospheric circulations associated with BSISO was different in September-October and November both near surface and in the mid-troposphere. (4) In November, the local atmospheric circulation associated with positive BSISO was the significant pressure gradient between an anti-cyclonic and a cyclonic circulation (Figure R4), which **weakened the release of the surface heat flux and did not maintain the negative SST anomalies in November.**

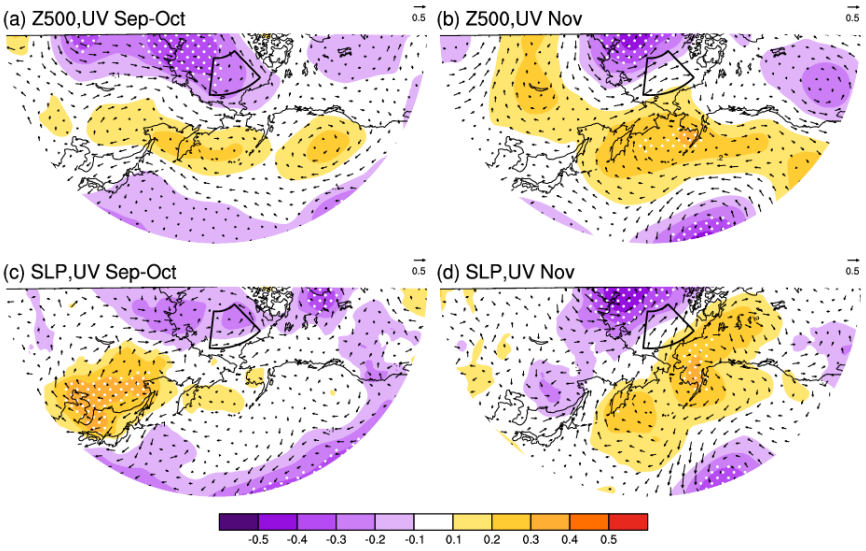

Figure R4. The CC between BSISO and September-October (a) geopotential height (shading), wind (arrow) at 500 hPa, (c) SLP (shade), and surface wind (arrow); and November (b) geopotential height (shading), wind (arrow) at 500 hPa, (d) SLP (shade), and surface wind (arrow) from 1979 to 2015, after detrending. The white dots indicate CCs exceeding the 90% confidence level (t test). The black box in (a–d) represents the location of the Beaufort Sea.

31. Line 118, why authors cannot directly link the SST anomalies over BS and GA to HDJ?

Reply:

Detailed comments 31 was similar with the Major comment 1.

Certainly, there was directly link between the November SST anomalies and the number of haze days in December and January. There are two reasons why we link the number of haze days and the September-October sea ice. (1) As an efficient driver, the September-October sea ice was one month in advance of the November SST, which **supports sufficient time gap to make the seasonal prediction in the real-time operation.** That is, in November, we may gain the sea ice September-October data and run the statistical seasonal prediction models. (2) The goal of this manuscript is to reveal the connection between the sea ice and the haze pollution in the early winter. Our studies **not only reveal the link between the SST and haze, but also deepen the understanding the impacts of the sea ice on the haze** by taking the SST anomalies as a bridge.

Response of Early Winter Haze ~~Days~~ in the North China Plain to Autumn Beaufort Sea Ice

Zhicong Yin [12], Yuyan Li[1] Huijun Wang[12]

[1]Key Laboratory of Meteorological Disaster, Ministry of Education / Joint International Research Laboratory of Climate and Environment Change (ILCEC) / Collaborative Innovation Center on Forecast and Evaluation of Meteorological Disasters (CIC-FEMD), Nanjing University of Information Science & Technology, Nanjing 210044, China

[2]Nansen-Zhu International Research Centre, Institute of Atmospheric Physics, Chinese Academy of Sciences, Beijing, China

Correspondence to: Yuyan Li (yyan370@163.com)

Abstract. Recently, early winter haze pollution in the North China Plain has been serious and disastrous, dramatically damaging human health and the social economy. In this study, we emphasized the close connection between the number of haze days in early winter ~~haze days~~ in the North China Plain and the September-October sea ice in the west of the Beaufort Sea (R=0.51) via both the observational analyses and numerical experiments. Due to efficient radiative cooling, the responses of atmospheric circulations partially manifested as reductions of surface wind speed over the Beaufort Sea and Gulf of Alaska, resulting in a warmer sea surface in the subsequent November. The sea surface temperature anomalies over the Bering Sea and Gulf of Alaska acted as a bridge. The warmer sea surface efficiently heated the above air and led to suitable atmospheric backgrounds to enhance the potential of haze weather (e.g., a weaker East Asia jet stream and a Rossby wave-like train propagated from North China and the Japan Sea, through the Bering Sea and Gulf of Alaska, to the Cordillera Mountains). Near the surface, the weakening sea level pressure gradient stimulated anomalous southerlies over the coastal area of China and brought about a calm and moist environment for haze formation. The thermal inversion was also enhanced to restrict the underswing of clear and dry upper air. Thus, the horizontal and vertical dispersion were both limited, and the fine particles were apt to accumulate and cause haze pollution.

Keywords: Haze, Pollution, Aerosol, Sea ice, Arctic, Climate change

1. Introduction

~~In February 2018, the highest temperature near the Arctic region was above the freezing point (Jason, 2018), raising tremendous concerns from global climate change scientists.~~ During the past few years, the increase of surface air temperature has been distinctly amplified in the Arctic ~~area~~ region~~(i.e., the Arctic Amplification feature)~~ and approximately twice as large as the average increase in global warming, which was called the Arctic Amplification (Zhou, 2017). ~~Recently, the~~ Arctic sea ice (ASI) decrease~~d~~ rapidly ~~due to the Arctic Amplification and reached a record low in September 2012~~since the satellite era, in particular, after the year of 2000 (Gao et al., 2015). The ~~loss~~ change of ASI, associated with

changed ~~the~~ reflection of solar radiation and ~~the~~ exchange of energy and fresh water, ~~which~~ could remotely connect with the climate in the Northern Hemisphere, especially the winter climate ~~variability~~ in Eurasia (Liu et al., 2007; Wang and Liu, 2016). ~~As an efficient external driver in the high latitudes, t~~The decreased ASI over the Barents–Kara Seas in late autumn stimulated a planetary-scale Rossby wave train in early winter (Honda et al., 2009; Kim et al., 2014) and transported its impacts to Eurasia. The variation of the autumn ASI had significant impacts on the East Asian jet stream and the East Asian trough (Li and Wang, 2013) as well as the winter Arctic Oscillation (Li and Wang, 2012; Li et al., 2015) and the East Asian winter monsoon (Li and Wang, 2014; Li et al., 2014). Since 2000, the snowfall in Siberia has been enhanced, which is probably related to the increased moisture flux from the Arctic (Cohen et al., 2012; Li and Wang, 2013). Liu et al. (2012) illustrated that the decrease of autumn ASI resulted in more blocking patterns and water vapor, which was a benefit for heavy snowfall in Europe during early winter and in the United States during winter. Furthermore, under the positive Pacific decadal oscillation phase, the autumn ASI reduction contributed to the subseasonal variability of surface air temperature in the East Asian winter (Xu et al., 2018; He, 2015). The dust (dry particles suspended in air after strong wind) and sandstorm (strong wind carrying sands) over North China, types of weather that are sensitive to wind, also showed close relationships with the variation of ASI after the mid-1990s (Fan et al., 2017). The sea ice over the Barents–Kara Seas induced dust-related atmospheric circulations (e.g., a strengthened East Asian jet, increased cyclogenesis, and greater atmospheric thermal instability).

Haze (polluted particulate aerosols suspended in air), also being sensitive to wind, frequently occurred under calm and static weather conditions, i.e., small surface winds and strong thermal inversion (Yin et al., 2015; Ding and Liu, 2014; Chen and Wang, 2015; Cai et al., 2017; Gao and Chen, 2017). For the long-term trend of number of haze days, human activities are the recognized and fundamental driver (Li et al., 2018; Yang et al., 2016; Chen et al., 2018; Zhang et al., 2018), but the rapid ASI decline also contributed to the trend of number of haze days~~haze pollution~~ in the North China Plain after 2000 (Wang and Chen 2016~~7~~). For the interannual to interdecadal variations, the impacts of ASI on the number of haze days~~haze~~ in the east of China were emphasized by observational analyses (Wang et al., 2015) and numerical studies (Li et al., 2017). By the sensitive experiments, Li et al. (2017) emphasized the impacts of ASI anomalies on haze pollution in North China, but deemphasized the role of ENSO (He et al., 2019). From 1979–2012, the ASI loss led to a northward shift of the East Asia jet stream and weak East Asian winter monsoons, indicating a strongly negative correlation with the number of haze days~~haze~~ in the east of China (Wang et al., 2015). However, the first mode of the Empirical Orthogonal Function (EOF) in Yin and Wang (2016a) presented different variations of number of haze days~~haze days~~ in the south and north of the Yangtze River. The positive relationship between the autumn sea ice in the Beaufort Sea and the number of haze days in winter~~ haze days~~ was briefly revealed without sufficient physical explanations but contributed to the prediction of number of haze days in winter~~ haze days~~ (Yin and Wang, 2016b, 2017b). The number of haze days in early winter (December-January) ~~haze days~~

also varied differently with that ine February ~~haze days~~ (figure omitted), ~~indicating a variant modulating mechanism from the climate drivers~~suggesting a potential different driving mechanism. Thus, an open question still existed, i.e., the connections between Beaufort Sea ice (BSI) and the number of haze days in early winter ~~haze pollution~~ in the North China Plain (NCP: 34–42°N, 114°E–120°E) and the associated physical mechanisms.

2. Datasets and methods

The monthly sea ice concentrations (1°×1°) were downloaded from the Met Office Hadley Center (Rayner et al., 2003), which is widely used in the sea ice-related analysis. The number of haze days~~haze days~~ were mainly calculated with the 6-hr observed visibility and relative humidity. The observed relative humidity, visibility, wind speed, and weather phenomena data used here were collected and controlled by the National Meteorological Information Center, China Meteorological Administration. The computing method of haze days was in accordance with Yin et al. (2017). That is, if the visibility was lower than 10km and the relative humidity was drier than 90%, the day was defined as one haze day after filtering the other weather affected visibility (i.e., precipitation, dust, sandstorm, etc.). The hourly $PM_{2.5}$ concentration data were provided by the Ministry of Environmental Protection of China, including 162 sites in the North China. The daily maximum $PM_{2.5}$ was the maximum value obtained over 24-hour measurements. The 1°×1° ERA-Interim data used here included the geopotential height (Z), zonal and meridional wind, specific humidity, vertical velocity, air temperature at different pressure levels, sea level pressure (SLP), boundary layer height and surface air temperature data (Dee et al., 2011). The monthly mean sea surface temperature (SST) datasets, with a horizontal resolution of 1°×1°, were also derived from the website of ERA-Interim (Dee et al., 2011). The 2.5°×2.5° monthly reanalysis heat fluxes (i.e., the sensible heat net flux and the latent heat net flux) were available on the website of the National Center for Environmental Prediction and the National Center for Atmospheric Research (Kalnay et al., 1996). The simulations from the Community Earth System Model Large Ensemble (CESM-LE) datasets are employed (Kay et al., 2015). There are 35 member ensembles in the CESM-LE simulations that completed at NCAR, with a horizontal resolution of 0.9° latitude × 1.25° longitude and 30 vertical levels. The CESM-LE simulations were completed by the fully coupled CESM model.

3. Variation of the early winter haze

In most of the observational sites in the east of China, the number of haze days in December and January (HDJ) accounted for more than 70% of the total number of haze days in winter ~~haze days~~ (Figure 1), indicating that the haze pollution in the early winter was more serious than that in February. Yin et al. (2018) also illustrated that the inter-annual variation of number of haze days~~haze days~~ in February was different from that in the early winter. Thus, it is necessary to analyze the features of haze pollution in the early winter and associated climate drivers. The observational HDJ were

decomposed by the EOF method and the variation contribution of the first and second modes were 33% and 14%, respectively. In the first mode, the HDJ in the south and north of the Yangtze River varied differently (Figure 1) and should have a distinguishing relationship with the autumn ASI. In this study, we focused on the HDJ in the NCP region (HDJ_{NCP}, i.e., mean of the 38 sited HDJ) and its connection with the autumn ASI.

The HDJ_{NCP} ~~varied approximately 30 days from~~was stable during 1979 to 1992 and decreased ~~slightly~~ from 1993 to 200~~7~~9. ~~Since~~ After 200~~8~~9, the ~~inter-annual variation of~~ HDJ_{NCP} ~~has~~ showed a strong upward trend.~~become more evident.~~ The minimum HDJ_{NCP} occurred in 2010, which was 17.5 days. Afterwards, the HDJ_{NCP} increased dramatically and persistently, reaching a maximum (i.e., 42.7 days) in 2015. The mass concentration of $PM_{2.5}$ is an important indicator of haze pollution. The daily maximum of area-mean $PM_{2.5}$ in 2015 is shown in Figure 2b and was above 100 μg/m³. The ~~synoptic processes of haze~~ concentrations of $PM_{2.5}$ were relatively ~~weaker~~lower in January 2016 than those in December but still exceeded the threshold of pollution in China (i.e., 75 μg/m³). On 23 December, the most disastrous haze occurred, and the area-mean $PM_{2.5}$ concentration approached 500 μg/m³, indicating quite poor air quality and a serious health risk.

4. Connection with ASI and associated physical mechanisms

As illustrated by Wang et al. (2015), the autumn ASI significantly and negatively affected the haze pollution in the east of China by modulating the large-scale atmospheric circulations and local meteorological conditions. Furthermore, the opposite pattern of number of haze days~~haze days~~ in the east of China was revealed in Figure 1. To confirm the response of HDJ_{NCP} to the autumn sea ice, the correlation coefficients between the HDJ_{NCP} and the September-October sea ice were assessed after removing the linear trend~~and are shown in~~ (Figure 3). A positive correlation was found from the East Siberian Sea to the Beaufort Sea. In this broad region, the significantly correlated area was intensively located over the west of the Beaufort Sea. Thus, the area-averaged September-October sea ice area over the west of the Beaufort Sea (73–80 °N, 146 °W–178 °W) was calculated and denoted as the BSISO index, whose correlation coefficient with HDJ_{NCP} was 0.51 (above the 99% confidence level) after removing the linear trend. This apparent positive relationship indicates that the efficient accumulation of the preceding autumn sea ice over the west of the Beaufort Sea significantly intensified the number of haze days in early winter ~~haze pollution~~ over the NCP area. To confirm this connection, the year-to-year change of the sea ice concentration was examined (Figure 4). From 1979 to 2015, there were seven years with significantly negative BSISO (i.e., BSISO<–0.8×its standard deviation), and ten years with significantly positive BSISO (i.e., BSISO>0.8×its standard deviation). During 65% of these years, the significant BSISO anomalies corresponded ~~induced~~ HDJ_{NCP} anomalies with the same mathematical sign. There were no significantly opposite responses of HDJ_{NCP} ($|HDJ_{NCP}| > 0.8\times$its standard deviation) to the BSISO anomalies. Furthermore, the relationship seemed to be enhanced after the mid-1990s. The same mathematical signs of the anomalies appeared more frequently. ~~, and the intensity of the responses was also amplified.~~

The ~~heavy~~ positive sea ice anomalies, with high albedo, can efficiently reflect solar radiation and restore more fresh water, which could influence the local and adjacent SST. The correlation coefficients between BSISO and the simultaneous and subsequent SST were computed (Figure 5). Because of efficient reflections of the solar radiation, the locally negative SST anomalies, located near the west of the Beaufort Sea (70–81 °N, 166 °E–138 °W), were ~~induced by~~associated with the ~~heavy~~ positive BSISO anomalies in October. In the following two months, these negative SST anomalies could not be sustained, i.e., these anomalous responses disappeared in November. However, the ~~induced~~ positive SST anomalies in the Bering Sea (49–60~~-~~ °N, 165 °W–180 °W) and the Gulf of Alaska (40–52 °N, 130 °W–165 °W) appeared in October and were persistently enhanced in November and December. These three significantly correlated SSTs, located near the west of the Beaufort Sea (WB), over the Bering Sea (BS) and the Gulf of Alaska (GA), were defined as SST_{WB}, SST_{BS} and SST_{GA}, respectively. The correlation coefficients between these three indices were enumerated in Table 1 to present the change of the correlationship with SST. Over time, the linkage between BSISO and local SST (i.e., SST_{WB}) rapidly receded. To confirm the role of the local SST on the HDJ_{NCP}, the correlation coefficient between HDJ_{NCP} and SST_{WB} was –0.30 in October (exceeding the 95% confidence level), and –0.05 and –0.10 in the following November and December (insignificant). However, the correlation coefficients between the SST_{BS} (SST_{GA}) and BSISO were persistent and even became enhanced in November and December (Table 1). We speculated that the November SST_{BS} and SST_{GA} was the junction between the BSISO and HDJ_{NCP}.

According to the numerical results illustrated by Deser and Tomas (2007), the responses of atmospheric circulations to sea ice anomalies were initially baroclinic in the first 5–10 days and progressively became more barotropic and increased in both spatial extent and magnitude within 2 months. In September and October, due to the radiative cooling of the ~~heavy~~ positive BSISO anomalies, the baroclinic responses of the atmospheric circulations manifested mainly as anomalous cyclonic circulation in the upper troposphere (Figure 6a). There were also weak anti-cyclonic responses in the Bering Sea and Gulf of Alaska. In the subsequent November, the extent of these ~~induced~~ cyclonic and anti-cyclonic anomalies increased, especially the anti-cyclonic circulations over the Bering Sea and Gulf of Alaska (Figure 6b). The barotropic structure of the atmospheric responses became more obvious, i.e., there were also cyclonic and anti-cyclonic circulations on both sides of the Beaufort Sea, near the surface (Figure 6d). In addition, there were also positive SLP anomalies near the Aleutian Islands, indicating a weak Aleutian Low. Near the surface, a significant anomalous southerly was ~~induced~~ existed between cyclonic and anti-cyclonic circulations, and an anomalous east wind was excited in the south of the anti-cyclonic circulation (Figure 6d). Overlapping with the climate mean state, the surface wind speeds over the RS1 (41–54 °N,140 °W–165 °W) and RS2 (70–76 °N,140 °W–170 °W) regions were significantly receded (Figure 7). The area-average surface wind speed was then calculated and denoted as $WSPD_{RS1}$ and $WSPD_{RS2}$ to examine its impacts on the simultaneous SST. In November, the climatological northeasterly through the Bering Strait transported cold seawater from the Arctic to the Bering Sea and

resulted in a lower SST. The correlation coefficient between $WSPD_{RS2}$ and SST is shown in Figure 8 and was significantly negative in the Bering Sea. The driver of the cold seawater transportations, i.e., the surface wind, decreased and led to warmer SST_{BS} in November. Another reduction of surface wind speed, i.e., $WSPD_{RS1}$, indicated the weakening of the west surface wind and accompanying subdued evaporation near the sea surface. This RS1 region was located consistently with the warmer Gulf of Alaska. The correlation coefficients between the $WSPD_{RS1}$ and SST_{GA} were significantly negative, indicating that the reduction of $WSPD_{RS1}$ resulted in a warmer sea surface over the Gulf of Alaska (Figure 9a). Due to the weakening of the water evaporation, the latent heat release slowed down both in the Bering Sea and the Gulf of Alaska, which conserved more thermal energy in the sea surface (Figure 9b). In addition, the upper anti-cyclonic circulations, with clear sky, facilitated more shortwave solar radiation onto the sea surface. The absorbed and stored thermal energy, which was connected with the ~~heavy~~ positive BSISO anomalies, heated the sea surface over the Gulf of Alaska in November, i.e., positive SST_{GA} anomalies. Both of the SST_{GA} and SST_{BS} were significantly influenced by the BSISO and synchronously changed (figure omitted). Thus, the SST_{BS} and SST_{GA} were integrated as SST_{BA} to analyze their corporate impacts on the HDJ_{NCP}. The variations of November SST_{BA} and the BSISO were strongly consistent, especially after 2000 (Figure 10). As presented in Table 1, from October, the SST_{BA} began to significantly connect with the BSISO. Over time, this connection persisted and strengthened. The correlation coefficient between November (December) SST_{BA} and the BSISO was 0.43 (0.48), exceeding the 99% significance test.

Statistically, the November SST_{BA} was significantly correlated with the HDJ_{NCP} (i.e., the correlation coefficient was 0.61 and above the 99% confidence level), showing strong impacts on the number of haze days in early winter ~~haze pollution~~ over the NCP region. To reveal the physical processes, the associated atmospheric circulations and local meteorological conditions were diagnosed in Figures 11–15. The warmer sea surface efficiently heated the above air and resulted in ascending motion from the Gulf of Alaska to the Aleutian Islands, which could extend to the atmosphere at 200 hPa (Figure 11). Furthermore, significant accompanying descending motions at 200 hPa were stimulated from the Sea of Okhotsk to the Hawaiian Islands (Figure 11a). Near the surface, there was also a sinking motion over the Hawaiian Islands (Figure 11b). On the mid-troposphere, the significantly negative Z500 anomalies, i.e., cyclonic circulations, were exerted above the warmer Bering Sea and Gulf of Alaska (Figure 12b). The responses of the December-January atmospheric circulations to the warmer November SST_{BA} showed deeply barotropic structures. There were also significant cyclonic circulations in the lower troposphere (Figure 12c) and near the surface (Figure 12d). At 500 hPa, there were significant anti-cyclonic anomalies located on both sides of the cyclonic circulations, i.e., over North China, the Japan Sea, and the Cordillera Mts. Thus, a Rossby wave-like train was induced by the SST_{BA}, which propagated from North China and the Japan Sea, through the Bering Sea and Gulf of Alaska, to the Cordillera Mts. This "+–+" pattern could also be recognized in the lower (Figure 12c) and upper (Figure 12a) troposphere. The anti-cyclonic circulations over North China and the Japan Sea were recognized as

the key atmospheric system to influence the haze pollution in the NCP area (Yin and Wang, 2016a; Yin et al., 2017). To confirm the linkage between this Rossby wave-like train and SST_{BA}, the area-averaged Z500 in three centers ([88 °E–115 °E, 30–50 °N], [150 °E–160 °W, 45–60 °N], [115 °W–130 °W, 50–60 °N]) were calculated and are shown in Figure 13. The correlation coefficients between the three centers, from west to east, with SST_{BA} were 0.47, –0.46, and 0.37, all above the 95% confidence level. Due to the change of the pressure gradient, there were positive zonal westerlies from Lake Baikal to the Hawaiian Islands and negative westerly anomalies from East China to the west subtropical Pacific (Figure 12a). Therefore, zonal west winds prevailed in the mid-high latitude, and the meridionality of the atmosphere was reduced. The East Asia jet stream was weakened by anomalous easterlies and shifted northwards, indicating the decrease of the southward cold air activities. In addition, the southern section of the East Asia major trough, which reached the NCP area and guided cold air southward, was truncated by the anomalous anti-cyclonic circulations (Figure 12b). In contrast, due to the cyclonic anomalies over the Aleutian area, the northern section of the East Asia major trough was enhanced but moved eastward. These large-scale anomalous atmospheric circulations could provide a suitable background for the enhancement of the potential of the haze weather (Yin and Wang, 2017a).

Near the surface, because of the SST_{BA} heating, the Aleutian Low moved eastward and was enhanced over the Bering Sea and Gulf of Alaska. Consistent with the barotropic anomalies in the above air, there were positive SLP anomalies from Northeast China to the west Pacific (Figure 12d). That is, a north-south seesaw over the North Pacific was discerned clearly, similar to the anomalous North Pacific Oscillation (NPO) pattern (Rogers, 1981). The difference of SLP ([140 °E–170 °W, 20–30 °N] minus [165 °E–155 °W, 48–65 °N]) was calculated to quantify this seesaw pattern, whose correlation coefficients with the BSISO, SST_{BA} and HDJ_{NCP} were 0.33, 0.64 and 0.61, respectively. Bounded by the east of China, the south positive center of NPO and the negative anomalies occupied the west Pacific and Eurasia, respectively. The drivers of the East Asian winter monsoon, i.e., the pressure gradient between the continent and the ocean, became weak, indicating the limitation of cold air and ventilation conditions. Compared to the local zonal wind, the meridional wind played more important roles on weakening the horizontal dissipation conditions of the air (Figure omitted). The ~~induced~~ southerly anomalies were located over the coastal area of China and transported moisture to the NCP area (Figure 14a), providing moist air for haze formation. In winter, the anomalous south winds also weakened the prevailing northerly and reduced the invasion of cold air. The humid atmosphere was conducive to the hygroscopic growth of pollutant particles, which reduced the visibility rapidly and structured stable weather conditions. The surface wind speed, indicating the horizontal dispersion capacity of the atmosphere, also subsided. In addition, the shallow thermal inversion layer or the boundary layer limited the upward dispersion of the pollutant particles. As shown in Figure 14b, the intensity of the thermal inversion over the NCP area was significantly heightened, while the boundary layer significantly declined. Generally, the air on the high altitude was relatively dry and clean. The sinking of the upper air to the surface was an important approach in dispersing the surface pollution (Sun et al.,

2017). Instead, the upward motion above the boundary layer resisted the breaking of the thermal layer and was in favor of haze occurrence (Figure 15a). The associated anomalous descending flow was blocked in the north of 46°N, which was consistent with the location of the northward cold air activities (Figure 15a). Influenced by the warmer SST_{BA}, there were anomalous ascending motions over the NCP area. Thus, the weakened downward transportation of momentum was not sufficient to enhance the winds near the surface and break the thermal inversion layer. Therefore, the clear, dry and cold air was difficult to transport to the surface, indicating the failure of the blowing wind. Under poor ventilation conditions, i.e., the horizontal and vertical dispersion was limited, the fine particles were apt to accumulate and cause haze pollution. Combined with favorable moisture conditions, the haze exacerbated rapidly and perniciously.

5. Causality verification by CESM-LE experiments

The connection between the haze pollution in North China and ASI, and associated physical mechanisms were statistically analyzed in the above sections. To confirm the causality, numerical experiments were designed with the public CESM-LE datasets. To be consistent with the observational results, the variables from CESM-LE from 1979 to 2015 are employed, which was combined by the historical simulation during 1979–2005 and the data during 2006–2015 from the future representative concentration pathway 8.5 forcing simulation. 35 CESM-LE ensemble members were used here. The CESM-LE simulations were completed by the fully coupled CESM model, thus the interactions among sea ice, sea temperature and atmosphere can be contained. The years when the sea ice anomalies concentrated in the west of the Beaufort Sea were selected and the differences between the positive BSISO and negative BSISO years were be identified as the responses to the sea ice anomalies. In the numerical experiment, all available CESM-LE members were included and different amplitudes of sea ice anomalies were composited, thus the uncertainty from the internal variability were largely reduced.

In Figure 16a, the sea ice anomalies were obvious in the key region. The maximum of the difference in sea ice concentration was more than 35% (Figure 16a). In the following November, the accumulated sea ice favored increased SST over the Gulf of Alaska (Figure 16b), which is in good accordance with the observed results. Although there were weaker, but negative SST responses in Bering Sea, the positive SST anomalies extended southwards and enhanced the air-sea interaction. In terms of the corresponding atmospheric circulations with regard to anomalous BSISO, the composite difference was also consistent with the observed results. The anti-cyclonic anomalies of the geopotential height at 500hPa were also well reproduced by the numerical model in the early winter (Figure 16c). On the lower troposphere, there were also anomalous anticyclone over North China and Northeast China, which induced anomalous southerlies (Figure 16d) and weakened the cold air from the high latitude. Furthermore, the moist air condition (Figure 16c) and lower boundary layer (Figure 16d) were also verified to be significantly connected with the positive BSISO anomalies. Consistent with the

observed results, the linkages between the BSISO and the haze pollution in the North China also exist in CESM-LE simulations. Meanwhile, the corresponding physical mechanisms were also well reproduced by the large ensemble members. The performances of numerical models in the mid-high latitude were consistently limited, however, the results from CESM-LE here successfully captured major features and general physical processes as expected. Consequently, the robustness of the proposed connections and physical mechanisms were strongly confirmed.

~~5.~~6. Conclusions and discussions

In the sub-seasonal scale, the haze weather in early winter occurred more frequently and varied differently from that in February. In this study, the close relationship between number of haze days in early winter ~~haze days~~ in the NCP area and the September-October sea ice in the west of the Beaufort Sea, with correlation coefficient = 0.51, was revealed. The ~~heavy~~ positive September-October sea ice anomalies over the west of the Beaufort Sea strongly intensified the early winter haze pollution over the NCP area, or more precisely, increased the number of haze days. Associated physical mechanisms were further examined. Due to the high albedo and efficient reflections, the local SST in October became cooler than the climate mean state, showing the radiative cooling effect. The responses of the atmospheric circulations initially manifested as anomalous cyclonic circulation in the upper troposphere, and then developed into cyclonic and anti-cyclonic circulations on both sides of the Beaufort Sea in the subsequent November. The decreased surface wind through the Bering Strait could not transport cold seawater to the Bering Sea as usual and led to a warmer sea surface over the Bering Sea. The reduction of surface wind speed over the Gulf of Alaska weakened the seawater evaporation and the latent heat release, which conserved more thermal energy in the sea surface, i.e., positive SST anomalies.

The November SST anomalies over the Bering Sea and Gulf of Alaska acted as a bridge in the close relationship between the BSISO (R=0.43, exceeding the 99% confidence level) and HDJ_{NCP} (R=0.61). The warmer sea surface efficiently heated the air above and resulted in significant responses in the atmosphere. In the upper-troposphere, zonal west wind anomalies prevailed in the mid-high latitudes, and the meridionality of the atmosphere was reduced, indicating the decrease of the southward cold air activities. A "+–+" Rossby wave-like train propagated from North China and the Japan Sea, through the Bering Sea and Gulf of Alaska, to the Cordillera Mts. Near the surface, the NPO-like pattern and the negative SLP anomalies over Eurasia induced southerly anomalies over the coastal area of China, providing a calm and moist environment for haze formation. In addition, the intensity of the thermal inversion over the NCP area was significantly enhanced, and the clear, dry and cold air was difficult to transport to the surface. The horizontal and vertical dispersions were both limited, so the fine particles were apt to accumulate and cause haze pollution. The linkages and corresponding physical mechanisms were well reproduced via the large CESM-LE ensembles, confirming the causality.

In this study, the response of the number of haze days in early winter ~~haze days~~ in the North China plain to the autumn Beaufort Sea ice and the associated physical mechanisms were investigated. As shown in Figure 2, the HDJ_{NCP} was 42.7 days and reached its maximum in 2015. Thus, the measurements in 2015 were composited after removing the linear trend to verify the results from the observational analyses (Figure 1~~6~~7). In September-October 2015, there were positive sea ice anomalies on the west of the Beaufort Sea (Figure 1~~6~~7a), which satisfied the close relationship revealed in this study. Meanwhile, an obviously warmer SST in November was observed in most of the BA region (Figure 1~~6~~7b), transferring the impacts of the BSISO. As a result, a weaker East Asia jet stream, an anomalous southerly (Figure 1~~6~~7c), limited horizontal and vertical dispersion conditions, and moist air (Figure 1~~6~~7d) enhanced the early-winter haze pollution in 2015. However, some questions remain unanswered and should be investigated with numerical models in future work. For example, the internal dynamic and thermal processes and how the ~~heavy~~ positive sea ice anomalies (radiative cooling) affected the atmospheric circulations, are not fully understood. During this work, linear correlation analyses were the main research technique, and the linear relationship was discovered. In fact, the dynamic–thermodynamic processes in the air-ice interaction are neither straightforward nor necessarily linear (Zhang et al., 2000; Gao et al., 2015). Considering the contradiction among the results by a single numerical model (Gao et al., 2015), a multi-model ensemble was required to solve the internal physical mechanisms. Furthermore, the November SST anomalies over the Bering Sea and Gulf of Alaska were treated as a bridge to connect the sea ice and the haze pollution. It is necessary to examine whether this bridge was constructed all the time. Particularly, after 2010, haze pollution became more serious. The driven role of the BSISO and the bridge of SST_{BA} needs to be verified. Moreover, as revealed by the EOF decomposition, the number of haze days in southern China varied differently. Its relationship with the sea ice in the Arctic is still unclear and needs to be addressed. The significant relationship revealed in this study and associated previous work potentially improved the monthly prediction of haze pollution. Valuable haze predictions are urgently needed by the scientific decision-making departments to control haze pollution in China (Wang, 2018).

Acknowledgements

This research was supported by the National Natural Science Foundation of China (41705058 and 91744311), the National Key Research and Development Plan (2016YFA0600703), the CAS–PKU Partnership Program, and the funding of the Jiangsu Innovation & Entrepreneurship team.

Reference

Cai, W. J., Li, K., Liao, H., Wang, H. J., Wu, L. X.: Weather Conditions Conducive to Beijing Severe Haze More Frequent under Climate Change, Nature Climate Change, doi:10.1038/nclimate3249, 2017.

Chen, H. P. and Wang, H. J.: Haze Days in North China and the associated atmospheric circulations based on daily visibility data from 1960 to 2012. J. Geophys. Res., 120, 5895–5909, doi:10.1002/2015JD023225, 2015.

Chen, H. P., Wang, H. J., Sun, J. Q., Xu, Y. Y., and Yin, Z. C.: Anthropogenic Fine Particulate Matter Pollution Will Be Exacerbated in Eastern China Due to 21st-Century GHG Warming, Atmos. Chem. Phys. Discuss., https://doi.org/10.5194/acp-2018-761, in review, 2018.

Cohen, J. L., Furtado, J. C., Barlow, M. A., Alexeev, V. A., Cherry, J. E.: Arctic warming, increasing snow cover and widespread boreal winter cooling, Environ Res Lett, 7:014007, 2012.

Dee, D. P., Uppala, S. M., Simmons, A. J., Berrisford, P., Poli, P., Kobayashi, S., Andrae, U., Balmaseda, M. A., Balsamo, G., Bauer, P., Bechtold, P., Beljaars, A. C. M.: The ERA-Interim reanalysis: configuration and performance of the data assimilation system. Q. J. Roy. Meteor. Soc., 137:, 553–597,doi:10.1002/qj.828, 2011.

Deser, C., Tomas, R. A., Peng, S.: The transient atmospheric circulation response to north atlantic sst and sea ice anomalies, Journal of Climate, 20(18), 4751, ~~1996~~2007.

Ding, Y. H., Liu, Y. J.: Analysis of long-term variations of fog and haze in China in recent 50 years and their relations with atmospheric humidity, Sci. China Ser. D: Earth Sci, 57:, 36–46 (in Chinese), 2014.

Fan, K., Xie, Z. M., Wang, H. J., Xu, Z. Q., Liu, J. P.: Frequency of spring dust weather in North China linked to sea ice variability in the Barents Sea, Climate Dynamics, doi: https://doi.org/10.1007/s00382-016-3515-7, 2017.

Gao, Y., Chen, D.: A dark October in Beijing 2016, Atmos. Oceanic Sci. Lett., 10 (3):), 206–213, 2017.

Gao, Y. Q., Sun J. Q., Li F., et al.: Arctic Sea Ice and Eurasian Climate: A Review, Adv. Atmos. Sci., 32(1):), 92–114, 2015.

He, C., Liu, R., Wang, X. M., Liu, S. C., Zhou, T. J., Liao W. H.: How does El Niño-Southern Oscillation modulate the interannual variability of winter haze days over eastern China? Science of the Total Environment, 651:, 1892–1902, https://doi.org/10.1016/j.scitotenv.2018.10.100, 2019.

He, S. P.: Asymmetry in the Arctic Oscillation Teleconnection with January Cold Extremes in Northeast China, Atmos. Oceanic Sci. Lett., 8(6), 386–391, doi: 10.3878/AOSL20150053, 2015.

Honda, M., Inoue, J., Yamane, S.: Influence of low Arctic sea ice minima on anomalously cold Eurasian winters, Geophys. Res. Lett., 36, L08707, doi: 10.1029/2008GL037079, 2009.

~~Jason, S.: Arctic temperatures soar 45 degrees above normal, flooded by extremely mild air on all sides, Washington Post, https://www.washingtonpost.com/news/capital-weather-gang/wp/2018/02/21/arctic-temperatures-soar-45-degrees-above-normal-flooded-by-extremely-mild-air-on-all-sides/?noredirect=on&utm_term=.ed2b94390646, Feb-22-2018.~~

Kalnay, E., Kanamitsu, M., Kistler, R., Collins, W., Deaven, D., Gandin, L., Iredell, M., Saha, S., White, G., Woollen, J., Zhu, Y., Leetmaa, A., Reynolds, R., Chelliah, M., Ebisuzaki, W., Higgins, W., Janowiak, J., Mo, K. C., Ropelewski, C., Wang, J., Jenne, R., Joseph, D.: The NCEP/NCAR 40-year reanalysis project, Bull. Am. Meteorol. Soc., 77:, 437–471, doi: 10.1175/1520-0477(1996)077<0437: TNYRP>2.0.CO; 2, 1996.

Kay, J. E., and Coauthors: The Community Earth System Model (CESM) Large Ensemble Project: A community resource for studying climate change in the presence of internal climate variability. Bull. Amer. Meteor. Soc., 96, 1333–1349, 2015.

Kim, B. M., Son, S. W., Min, S. K., Jeong, J. H., Kim, S. J., Zhang, X.D., Shim, T., Yoon, J. H.: Weakening of the

stratospheric polar vortex by Arctic sea-ice loss, Nature Communications, doi: 10.1038/ncomms5646, 2014.

~~Li, F., Wang, H. J., Gao, Y. Q.: On the strengthened relationship between East Asian winter monsoon and Arctic Oscillation: A comparison of 1950–1970 and 1983–2012. J.Climate, 27, 5075–5091, doi: 10.1175/JCLI-D-13-00335.1. 2014.~~

Li, F., Wang, H. J.: Autumn Eurasian snow depth, autumn Arctic sea ice cover and East Asian winter monsoon, Int. J. Climatol., doi: 10.1002/joc.3936 s, 2014.

Li, F., Wang, H. J.: Autumn sea ice cover, winter northern hemisphere annular mode, and winter precipitation in Eurasia, J. Climate, 26(11), 3968–3981, 2012.

Li, F., Wang, H. J.: Relationship between Bering sea ice cover and East Asian winter monsoon Year-to-Year Variations, Adv. Atmos. Sci., 30(1), 48–56, 2013.

Li, F., Wang, H. J., Gao, Y. Q.: On the strengthened relationship between East Asian winter monsoon and Arctic Oscillation: A comparison of 1950–1970 and 1983–2012. J.Climate, 27, 5075–5091, doi: 10.1175/JCLI-D-13-00335.1. 2014.

Li, F., Wang, H. J., Gao, Y. Q.: Change in Sea Ice Cover is Responsible for Non-Uniform Variation in Winter Temperature over East Asia. Atmos. Oceanic Sci. Lett., 8(6), 376–382, doi: 10.3878/AOSL20150039. 2015.

Li, K., Liao, H., Cai, W., Yang, Y.: Attribution of anthropogenic influence on atmospheric patterns conducive to recent most severe haze over eastern China, Geophys. Res. Lett., 45(4), 2072–2081, doi:10.1002/2017GL076570, 2018.

Li, S. L., Han, Z., Chen, H. P.: A Comparison of the Effects of Interannual Arctic Sea Ice Loss and ENSO on Winter Haze Days: Observational Analyses and AGCM Simulations, J. Meteor. Res., 31(5), 820–833, doi: 10.1007/s13351-017-7017-2, 2017.

Liu, J. P., Curry J. A., Wang, H. J., Song, M., Horton, R. M.: Impact of declining Arctic sea ice on winter snowfall, Proc. Natl. Acad. Sci. U.S.A., 109, 4074–4079, 2012.

Liu, J. P., Zhang, Z. H., Horton, R. M., Wang, C. Y., Ren, X. B.: Variability of North Pacific Sea Ice and East Asia North Pacific Winter Climate, J. Climate, 20, 1991–2001, doi:10.1175/JCLI4105.1, 2007.

Rayner, N. A., D. E. Parker, E. B. Horton, C. K. Folland, L. V. Alexander, D. P. Rowell, E. C. Kent, and A. Kaplan.: Global analyses of sea surface temperature, sea ice, and night marine air temperature since the late nineteenth century, J. Geophys. Res., 108, 4407, doi:10.1029/2002JD002670, 2003.

Rogers, J. C.: The North Pacific Oscillation, International Journal of Climatology, 1(1), 39–57. doi:10.1002/joc.3370010106, 1981.

Sun, X. C., Han Y. Q., Li, J., et al.: Analysis of the Influence of Vertical Movement on the Process of Fog and Haze with Air Pollution, Plateau Meteorology (in Chinese), 36(4), 1106–1114, 2017.

Wang, H. J., Chen, H. P., Liu J. P.: Arctic sea ice decline intensified haze pollution in eastern China, Atmos. Oceanic Sci. Lett., 8 (1): 1–9, 2015.

Wang, H. J., Chen, H. P.: Understanding the recent trend of haze pollution in eastern China: role of climate change, Atmos. Chem. Phys., 16, 4205–4211, 2016.

Wang, H. J.: On assessing haze attribution and control measures in China, Atmospheric and Oceanic Science Letters, 11, 2, 120–122, DOI: 10.1080/16742834.2018.1409067, 2018.

Wang, S. Y., Liu, J. P.: Delving into the relationship between autumn Arctic sea ice and central–eastern Eurasian winter climate, Atmos. Oceanic Sci. Lett., 9(5), 366–374, doi: 10.1080/16742834.2016.1207482, 2016.

Xu, X. P., Li, F., He, S. P., Wang, H. J.: Subseasonal reversal of East Asian surface temperature variability in winter 2014/15,

Adv. Atmos. Sci., 35(6), https://doi.org/10.1007/s00376-017-7059-5, 2018.

Yang, Y., Liao, H., Lou, S.: Increase in winter haze over eastern China in recent decades: Roles of variations in meteorological parameters and anthropogenic emissions, J. Geophys. Res. Atmos., 121~~:~~, 13050–13065, 2016.

Yin, Z. C., Wang, H. J.: The relationship between the subtropical Western Pacific SST and haze over North-Central North China Plain, International Journal of Climatology, 36~~:~~, 3479–3491, DOI: 10.1002/joc.4570, 2016a.

Yin, Z. C., Wang, H. J.: Seasonal prediction of winter haze days in the north central North China Plain, Atmos. Chem. Phys., 16, 14843-14852, https://doi.org/10.5194/acp-16-14843-2016, 2016b.

~~Yin, Z. C., Wang, H. J., Chen, H. P.: Understanding severe winter haze events in the North China Plain in 2014: roles of climate anomalies, Atmos. Chem. Phys., 17, 1641–1651, doi:10.5194/acp-17-1641-2017, 2017.~~

Yin, Z. C., Wang, H. J. Role of Atmospheric Circulations on Haze Pollution in December 2016, Atmos. Chem. Phys., 17, 11673-11681, doi: 10.5194/acp-17-11673-2017, 2017a.

Yin, Z. C., Wang, H. J.: Statistical Prediction of Winter Haze Days in the North China Plain Using the Generalized Additive Model, Journal of Applied Meteorology and Climatology, 56~~:~~, 2411–2419, DOI: https://doi.org/10.1175/JAMC-D-17-0013.1, 2017b.

Yin, Z. C., Wang, H. J., Chen, H. P.: Understanding severe winter haze events in the North China Plain in 2014: roles of climate anomalies, Atmos. Chem. Phys., 17, 1641–1651, doi:10.5194/acp-17-1641-2017, 2017.

Yin, Z. C., Wang, H. J., Guo, W. L.: Climatic change features of fog and haze in winter over North China and Huang-Huai Area, SCIENCE CHINA Earth Sciences, 58(8)~~:~~ 1370–1376, 2015.

Yin, Z. C., Wang, H. J., Ma, X. H.: Possible Linkage between the Chukchi Sea Ice in the Early Winter and the February Haze Pollution in the North China Plain, Climate Dynamics. under review, 2018.

Zhang, J. T., Rothrock, D., Steele, M.: Recent changes in Arctic sea ice: The interplay between ice dynamics and thermodynamics, J. Climate, 13, 3099–3314, 2000.

Zhang, Q. Q., Ma, Q., Zhao, B., et al.:~~,~~ ~~2018.~~ Winter haze over North China Plain from 2009 to 2016: Influence of emission and meteorology~~[J].~~, Environmental Pollution, 242~~:~~, 1308–1318, 2018.

Zhou, W.: Impact of Arctic amplification on East Asian winter climate, Atmos. Oceanic Sci. Lett., 10(5), 385–388, doi: 10.1080/16742834.2017.1350093, 2017.

Table and Figures captions

Table 1. The correlation coefficients (CC) between the BSISO (HDJ_{NCP}) and SST indices in October, November, and December. The linear trend was removed. '*' indicates that the CCs exceed the 95% confidence level, and '**' indicates that the CCs exceed the 99% confidence level. The meanings of the abbreviations were also explained.

Figure 1. The spatial pattern (shading) of the first EOF mode (variation contribution: 33%) for HDJ from 1979 to 2015. The black crosses and dots represent the locations of the observation stations. The cross (dot) indicated that the HDJ accounted for more (less) than 70% of the total winter haze days.

Figure 2. The variation of (a) HDJ_{NCP} from 1979 to 2015 and (b) daily maximum $PM_{2.5}$ from December to January in 2015 over the NCP area. The error bars in panel (a) represent one standard error among the measured sites.

Figure 3. The correlation coefficients (CC) between the HDJ_{NCP} and September-October sea ice concentration from 1979 to 2015, after detrending. The black dots indicate CCs exceeding the 95% confidence level (t test). The black box represents the selected Beaufort Sea.

Figure 4. Distributions of the September-October sea ice concentration after removal of the linear trend in typical years (i.e., the year when |BSISO|>0.8×its standard deviation). The "+" and "–" represent the mathematical sign of the BSISO and HDJ_{NCP} indices. The ".sig" indicates that the absolute value of the index anomaly was larger than 0.8×its standard deviation.

Figure 5. The CC between the BSISO and SST in (a) October, (b) November, and (c) December, from 1979 to 2015, after detrending. The black dots indicate CCs exceeding the 95% confidence level (t test). The black boxes (WB: west of Beaufort Sea, BS: Bering Sea and GA: Gulf of Alaska) are the significantly correlated areas, which were used to calculate the SST indices.

Figure 6. The CC between BSISO and September-October (a) geopotential height (shading), wind (arrow) at 500 hPa, (c) SLP (shade), and surface wind (arrow); and November (b) geopotential height (shading), wind (arrow) at 500 hPa, (d) SLP (shade), and surface wind (arrow) from 1979 to 2015, after detrending. The white dots indicate CCs exceeding the 90% confidence level (t test). The black box in (a–d) represents the location of the Beaufort Sea.

Figure 7. The distribution of the climate mean surface wind (arrow) in November and the CC between the BSISO and surface wind speed in November from 1979 to 2015, after detrending. The black dots indicate CCs exceeding the 95% confidence level (t test). The black boxes (RS1 and RS2) are the significantly correlated areas, which were used to calculate the $WSPD_{RS1}$ and $WSPD_{RS2}$ index.

Figure 8. The CC between $WSPD_{RS2}$ and SST in November from 1979 to 2015. The black dots indicate that the CCs exceeded the 95% confidence level (t test). The black box represents the BA area. The linear trend was removed.

Figure 9. The CC between $WSPD_{RS1}$ and (a) SST and (b) latent heat flux in November from 1979 to 2015. The black dots indicate that the CCs exceeded the 95% confidence level (t test). The black box represents the BA area. The linear trend was removed.

Figure 10. The variation of the normalized BSISO (blue) and November SST_{BA} (green) from 1979 to 2015, after detrending.

Figure 11. The CC between November SST_{BA} and (a) omega at 200 hPa, (b) at 1000 hPa in December and January from 1979 to 2015. The black dots indicate that the CCs exceeded the 95% confidence level (t test). The linear trend was removed. The black box represents the BA area.

Figure 12. The CC between the November SST_{BA} and (a) zonal wind at 200 hPa, (b) wind (arrow), geopotential height (shading) at 500 hPa, (c) wind (arrow), geopotential height (shading) at 850 hPa, (d) surface wind (arrow), and SLP (shading) in December-January from 1979 to 2015. The black dots indicate that the CCs exceeded the 95% confidence level (t test). The linear trend was removed. The black boxes in panel (b) represent the three anomalous centers at 500 hPa, and the gray

and black boxes in panel (d) represent the negative and positive anomalous centers.

Figure 13. The variation of the November normalized SST_{BA} (gray, bar) and area-averaged geopotential height at 500 hPa of the three anomalous centers (west: black, middle: green, east: orange) from 1979 to 2015, after detrending.

Figure 14. The CC between the November SST_{BA} and (a) surface wind (arrow), specific humidity (shading) at 1000 hPa (b) BLH (shading), thermal inversion potential (contour, solid (dashed) green lines indicate that the positive (negative) correlations exceeded the 90% confidence level (t test)) from 1979 to 2015. The black dots indicate that the CCs exceeded the 90% confidence level (t test). The linear trend was removed. The black boxes represent the NCP area. The thermal inversion potential was defined as the air temperature at 850 hPa minus SAT.

Figure 15. The cross-section (114 °E–120 °E mean) CC between (a) the HDJ_{NCP}, (b) November SST_{BA} and omega (shading), wind (arrow) in December-January from 1979 to 2015. The black dots indicate that the CCs exceeded the 95% confidence level (t test). The linear trend was removed.

Figure 16. Composite difference of (a) September-October sea ice concentration, (b) sea surface temperature in November, (c) geopotential height (contour) at 500 hPa, surface specific humidity in December-January, (d) BLH (shading), surface wind (arrow) in December-January. The black box in panel (a) represents the location of the Beaufort Sea, and in panel (b) it represents the BA area. Results are based on 35 ensembles of CESM-LE simulations. The black dots indicate that mathematical sign of the changes with shading from more than 50% of the members are consistent with the ensemble mean.

Figure 1~~6~~7. The distributions of (a) September-October sea ice concentration in 2015, (b) sea surface temperature in November 2015, (c) geopotential height (shading) at 500 hPa, wind (arrow) at 200 hPa in December-January 2015, (d) specific humidity (shading) at 1000 hPa, BLH (black dots indicate that its value is negative), WSPD (contour, solid black lines indicate a negative value) in December-January 2015. The black box in panel (a) represents the location of the Beaufort Sea, and in panel (b) it represents the BA area. The linear trend was removed.

Table 1. The correlation coefficient~~s~~ (CC) between the BSISO (HDJ_{NCP}) and SST indices in October, November, and December. The linear trend was removed. '*' indicates that the CCs exceed the 95% confidence level, and '**' indicates that the CCs exceed the 99% confidence level. The meanings of the abbreviations were also explained.

CC		Oct	Nov	Dec
BSISO: Beaufort Sea Ice in Sep-Oct	**SST_{WB}**: SST over the west of the Beaufort Sea	–0.75**	–0.26	–0.23
	SST_{BS}: SST over the Bering Sea	0.27	0.41*	0.45**
	SST_{GA}: SST over the Gulf of Alaska	0.31	0.40*	0.44**
	SST_{BA}: SST_{BS+} SST_{GA}	0.34*	0.43**	0.48**
HDJ_{NCP}: Haze days in Dec-Jan	**SST_{WB}**: SST over the west of the Beaufort Sea	–0.30	–0.05	–0.10
	SST_{BA}: SST_{BS+} SST_{GA}	0.52**	0.61**	0.56**

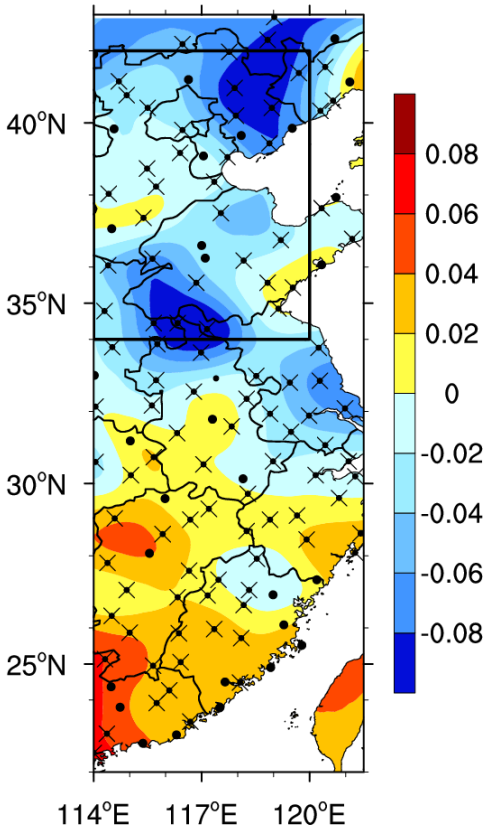

Figure 1. The spatial pattern (shading) of the first EOF mode (variation contribution: 33%) for HDJ from 1979 to 2015. The black crosses and dots represent the locations of the observation stations. The cross (dot) indicated that the HDJ accounted for more (less) than 70% of the total winter haze days.

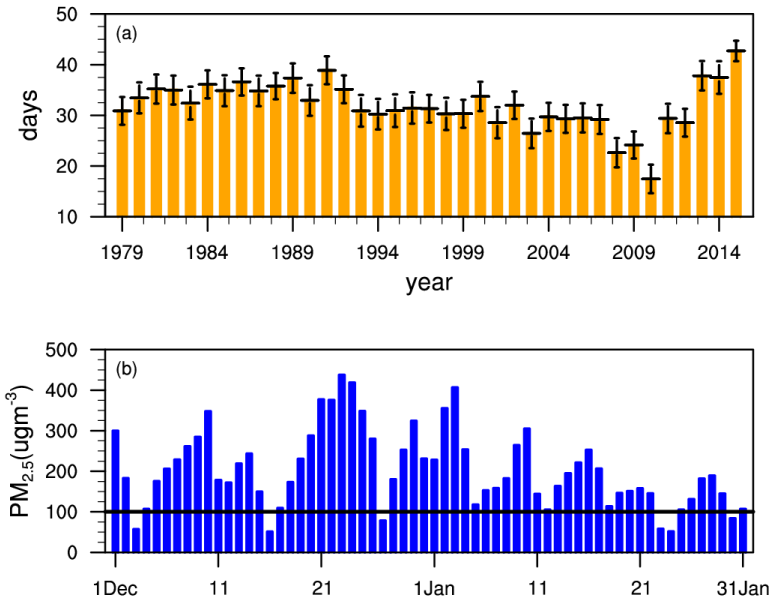

Figure 2. The variation of (a) HDJ_{NCP} from 1979 to 2015 and (b) daily maximum PM2.5 from December to January in 2015 over the NCP area. The error bars in panel (a) represent one standard error among the measured sites.

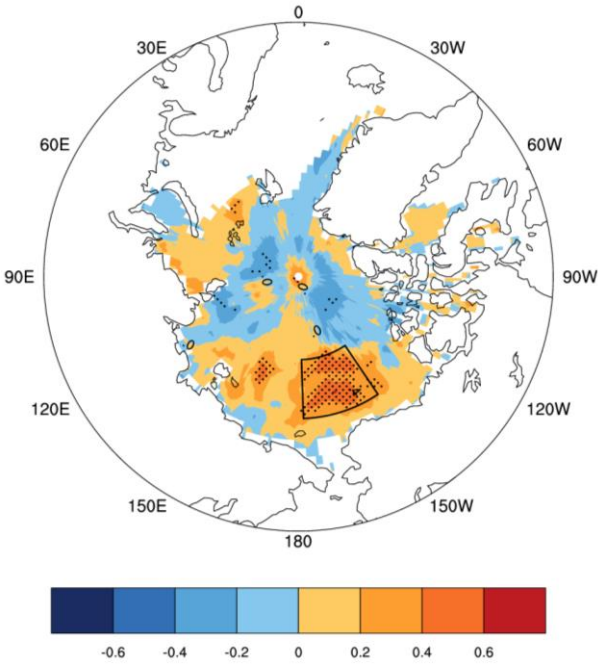

Figure 3. The correlation coefficients (CC) between the HDJ_{NCP} and September-October sea ice concentration from 1979 to 2015, after detrending. The black dots indicate CCs exceeding the 95% confidence level (t test). The black box represents the selected Beaufort Sea.

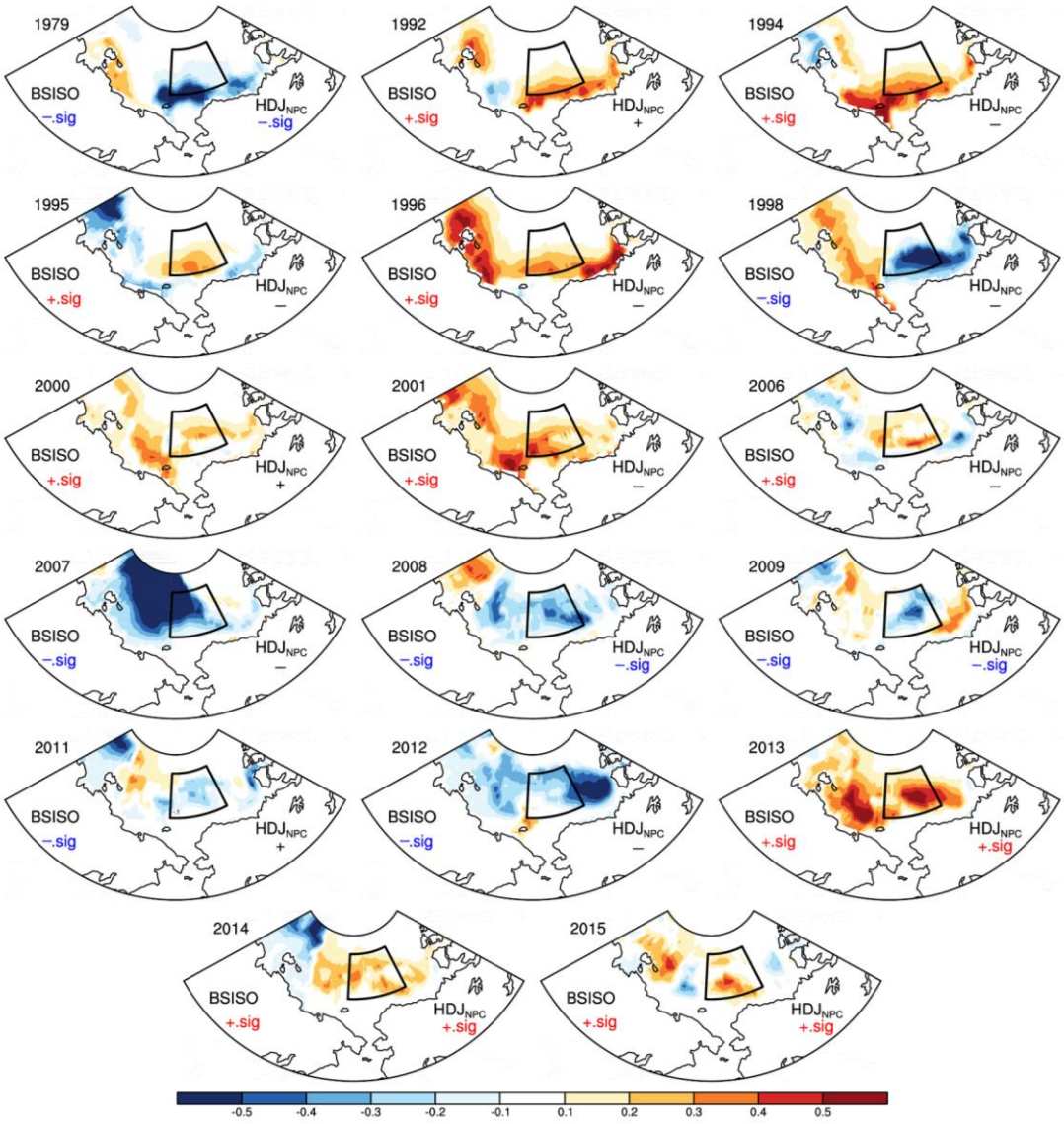

Figure 4. Distributions of the September-October sea ice concentration after removal of the linear trend in typical years (i.e., the year when |BSISO|>0.8 ×its standard deviation). The "+" and "–" represent the mathematical sign of the BSISO and HDJ_{NCP} indices. The ".sig" indicates that the absolute value of the index anomaly was larger than 0.8 ×its standard deviation.

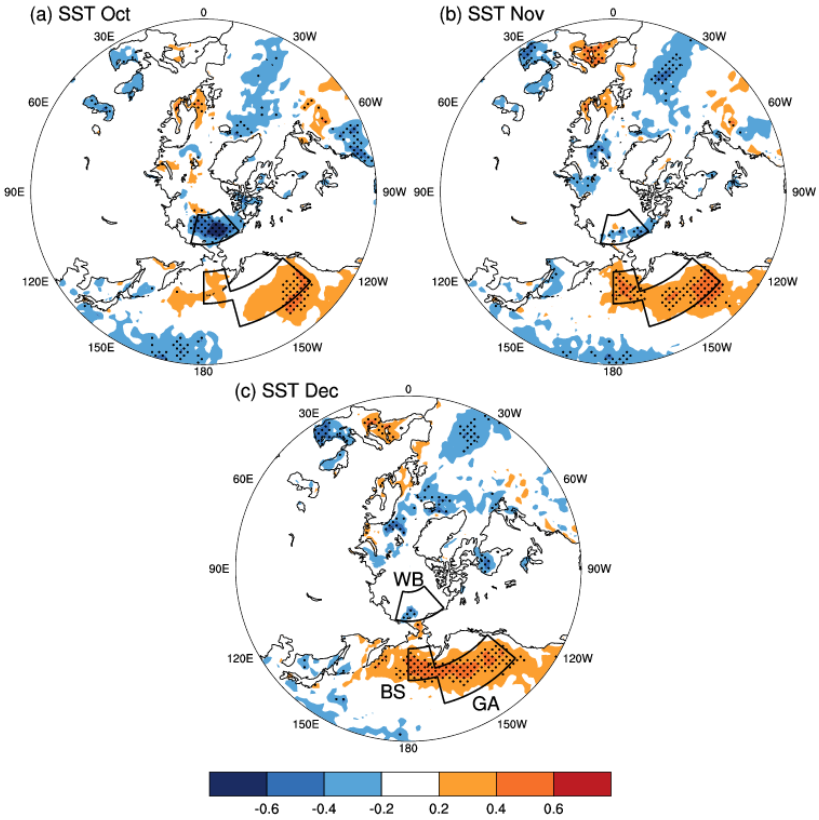

Figure 5. The CC between the BSISO and SST in (a) October, (b) November, and (c) December, from 1979 to 2015, after detrending. The black dots indicate CCs exceeding the 95% confidence level (t test). The black boxes (WB: west of Beaufort Sea, BS: Bering Sea and GA: Gulf of Alaska) are the significantly correlated areas, which were used to calculate the SST indices.

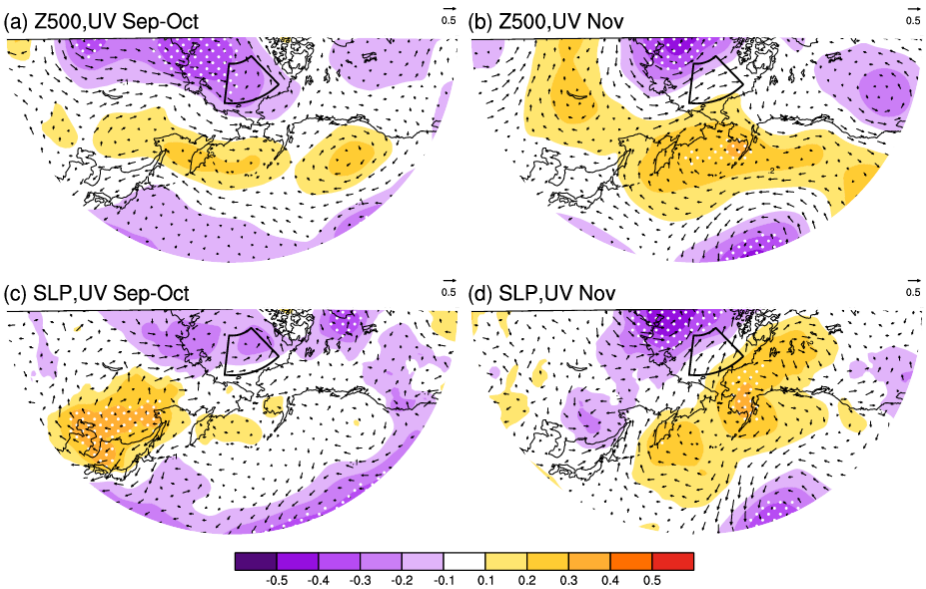

Figure 6. The CC between BSISO and September-October (a) geopotential height (shading), wind (arrow) at 500 hPa, (c) SLP (shade), and surface wind (arrow); and November (b) geopotential height (shading), wind (arrow) at 500 hPa, (d) SLP (shade), and surface wind (arrow) from 1979 to 2015, after detrending. The white dots indicate CCs exceeding the 90% confidence level (t test). The black box in (a–d) represents the location of the Beaufort Sea.

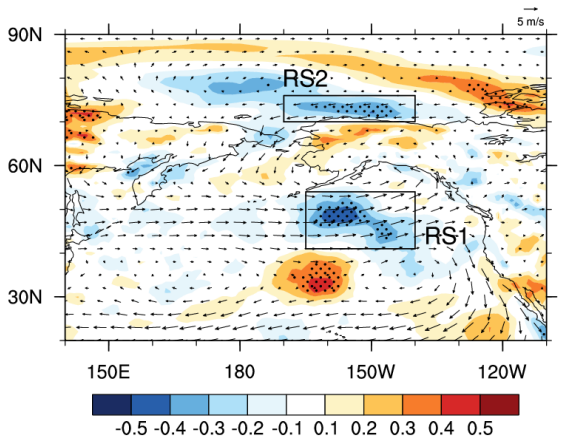

Figure 7. The distribution of the climate mean surface wind (arrow) in November and the CC between the BSISO and surface wind speed in November from 1979 to 2015, after detrending. The black dots indicate CCs exceeding the 95% confidence level (t test). The black boxes (RS1 and RS2) are the significantly correlated areas, which were used to calculate the $WSPD_{RS1}$ and $WSPD_{RS2}$ index.

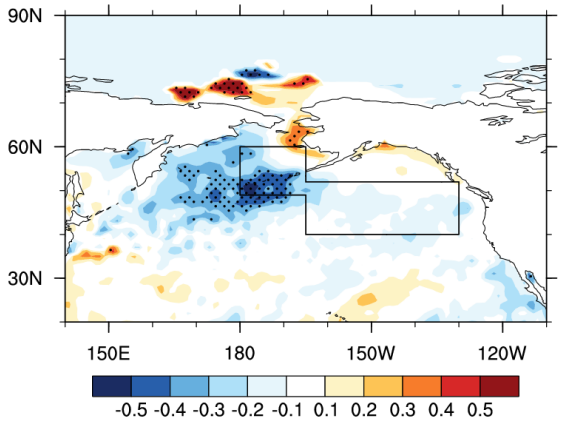

510

Figure 8. The CC between $WSPD_{RS2}$ and SST in November from 1979 to 2015. The black dots indicate that the CCs exceeded the 95% confidence level (t test). The black box represents the BA area. The linear trend was removed.

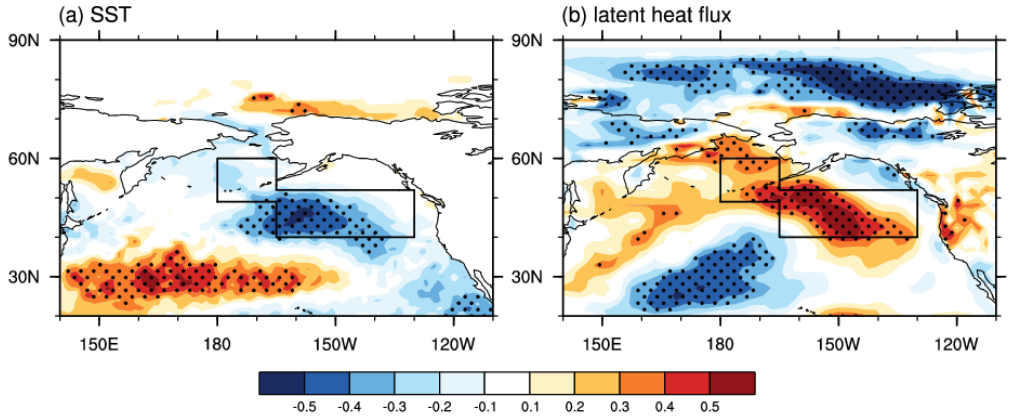

Figure 9. The CC between $WSPD_{RS1}$ and (a) SST and (b) latent heat flux in November from 1979 to 2015. The black dots indicate

515 **that the CCs exceeded the 95% confidence level (t test). The black box represents the BA area. The linear trend was removed.**

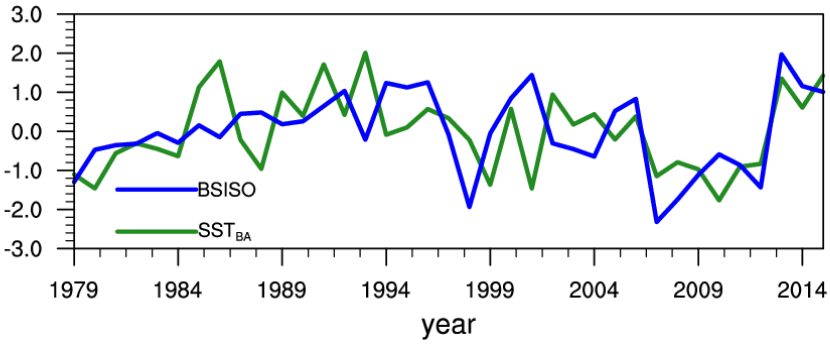

Figure 10. The variation of the normalized BSISO (blue) and November SST_{BA} (green) from 1979 to 2015, after detrending.

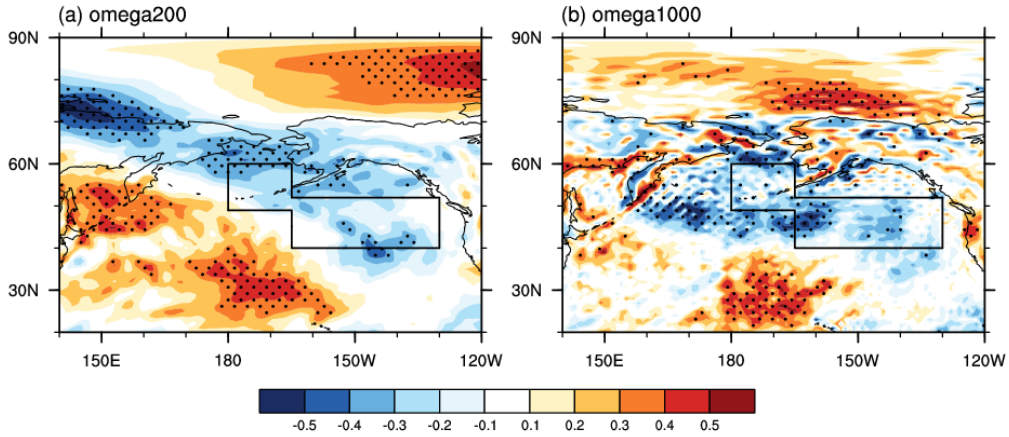

Figure 11. The CC between November SST_{BA} and (a) omega at 200 hPa, (b) at 1000 hPa in December and January from 1979 to 2015. The black dots indicate that the CCs exceeded the 95% confidence level (t test). The linear trend was removed. The black box represents the BA area.

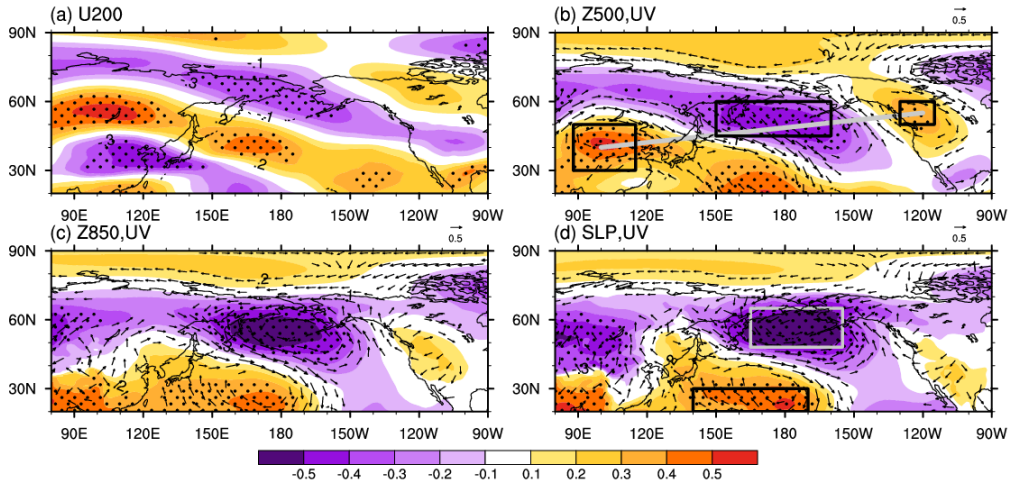

Figure 12. The CC between the November SST_{BA} and (a) zonal wind at 200 hPa, (b) wind (arrow), geopotential height (shading) at 500 hPa, (c) wind (arrow), geopotential height (shading) at 850 hPa, (d) surface wind (arrow), and SLP (shading) in December-January from 1979 to 2015. The black dots indicate that the CCs exceeded the 95% confidence level (t test). The linear trend was removed. The black boxes in panel (b) represent the three anomalous centers at 500 hPa, and the gray and black boxes in panel (d) represent the negative and positive anomalous centers.

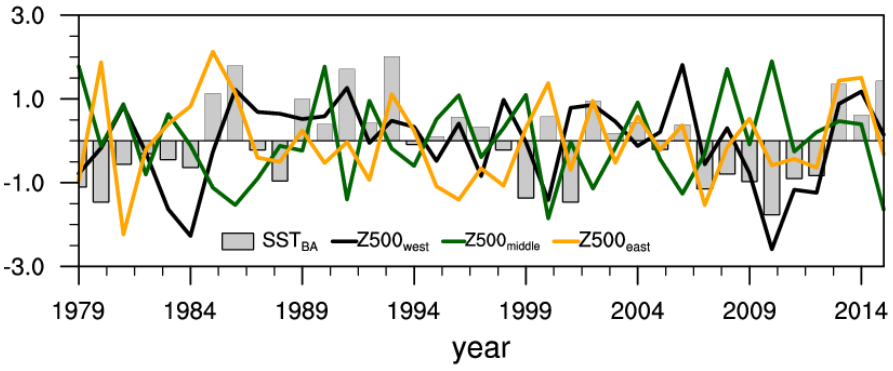

Figure 13. The variation of the November normalized SST_{BA} (gray, bar) and area-averaged geopotential height at 500 hPa of the three anomalous centers (west: black, middle: green, east: orange) from 1979 to 2015, after detrending.

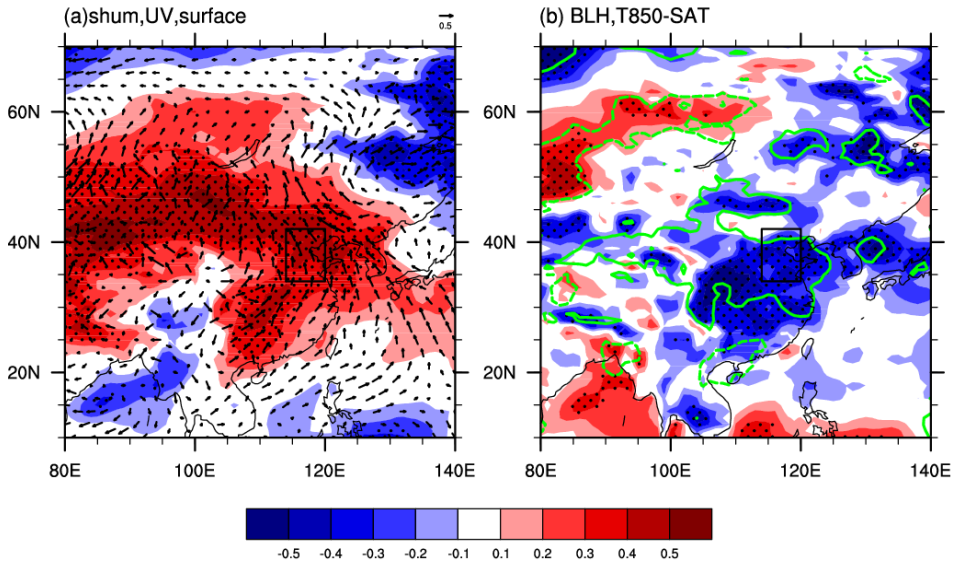

Figure 14. The CC between the November SST_{BA} and (a) surface wind (arrow), specific humidity (shading) at 1000 hPa (b) BLH (shading), thermal inversion potential (contour, solid (dashed) green lines indicate that the positive (negative) correlations exceeded the 90% confidence level (t test)) from 1979 to 2015. The black dots indicate that the CCs exceeded the 90% confidence level (t test). The linear trend was removed. The black boxes represent the NCP area. The thermal inversion potential was defined as the air temperature at 850 hPa minus SAT.

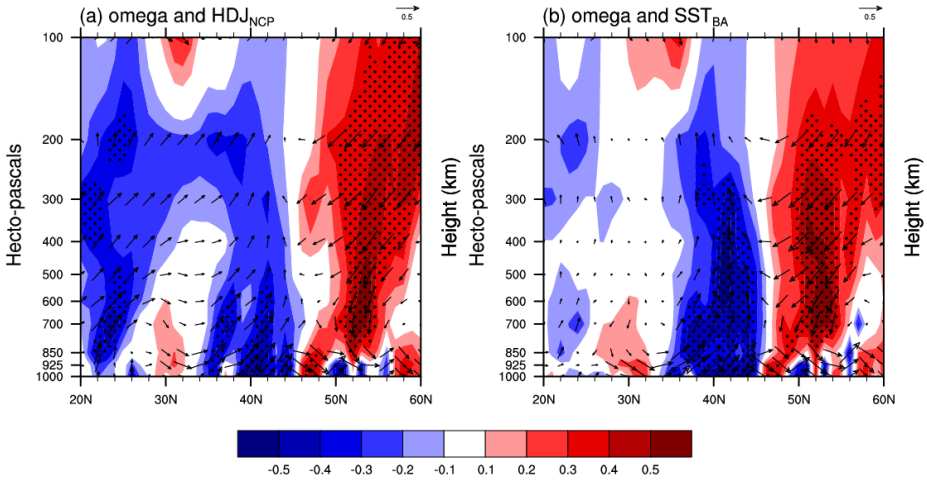

Figure 15. The cross-section (114 °E–120 °E mean) CC between (a) the HDJ_{NCP}, (b) November SST_{BA} and omega (shading), wind (arrow) in December-January from 1979 to 2015. The black dots indicate that the CCs exceeded the 95% confidence level (t test). The linear trend was removed.

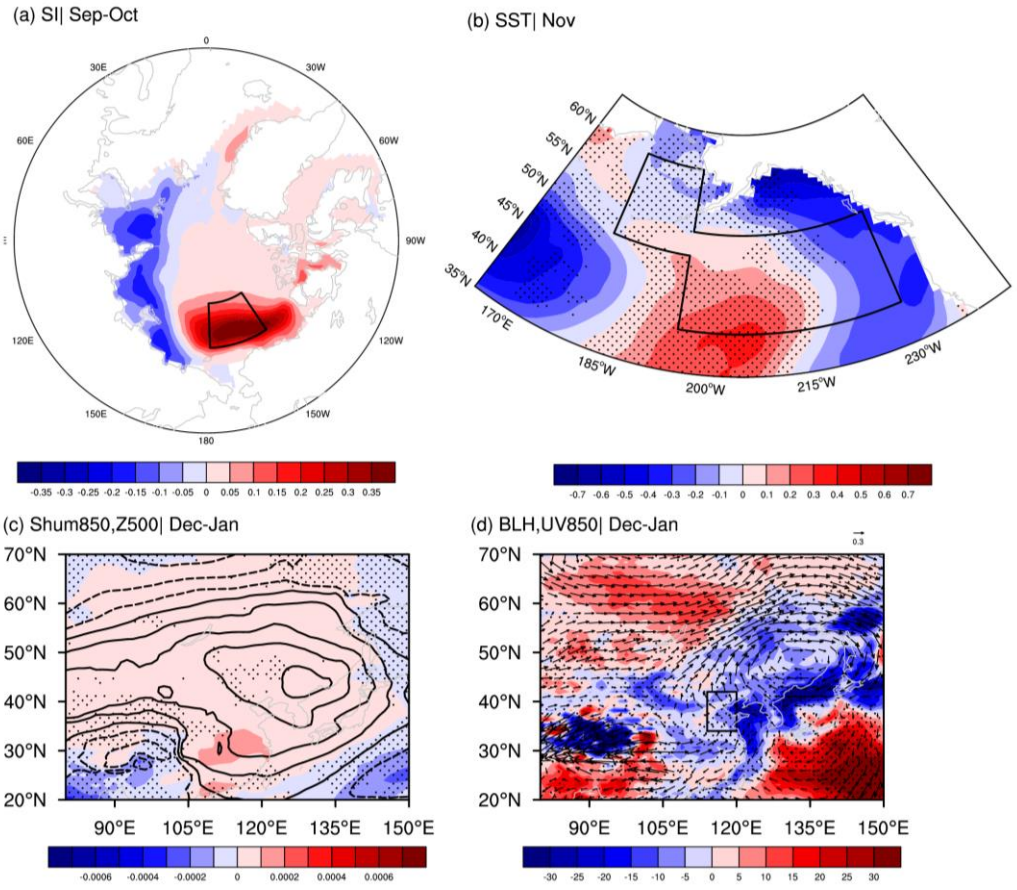

Figure 16. Composite difference of (a) September-October sea ice concentration, (b) sea surface temperature in November, (c) geopotential height (contour) at 500 hPa, specific humidity at 850 hPa in December-January, (d) BLH (shading), wind (arrow) at 850 hPa in December-January. The black box in panel (a) represents the location of the Beaufort Sea, and in panel (b) it represents the BA area. Results are based on 35 ensembles of CESM-LE simulations. The black dots indicate that mathematical sign of the changes with shading from more than 50% of the members are consistent with the ensemble mean.

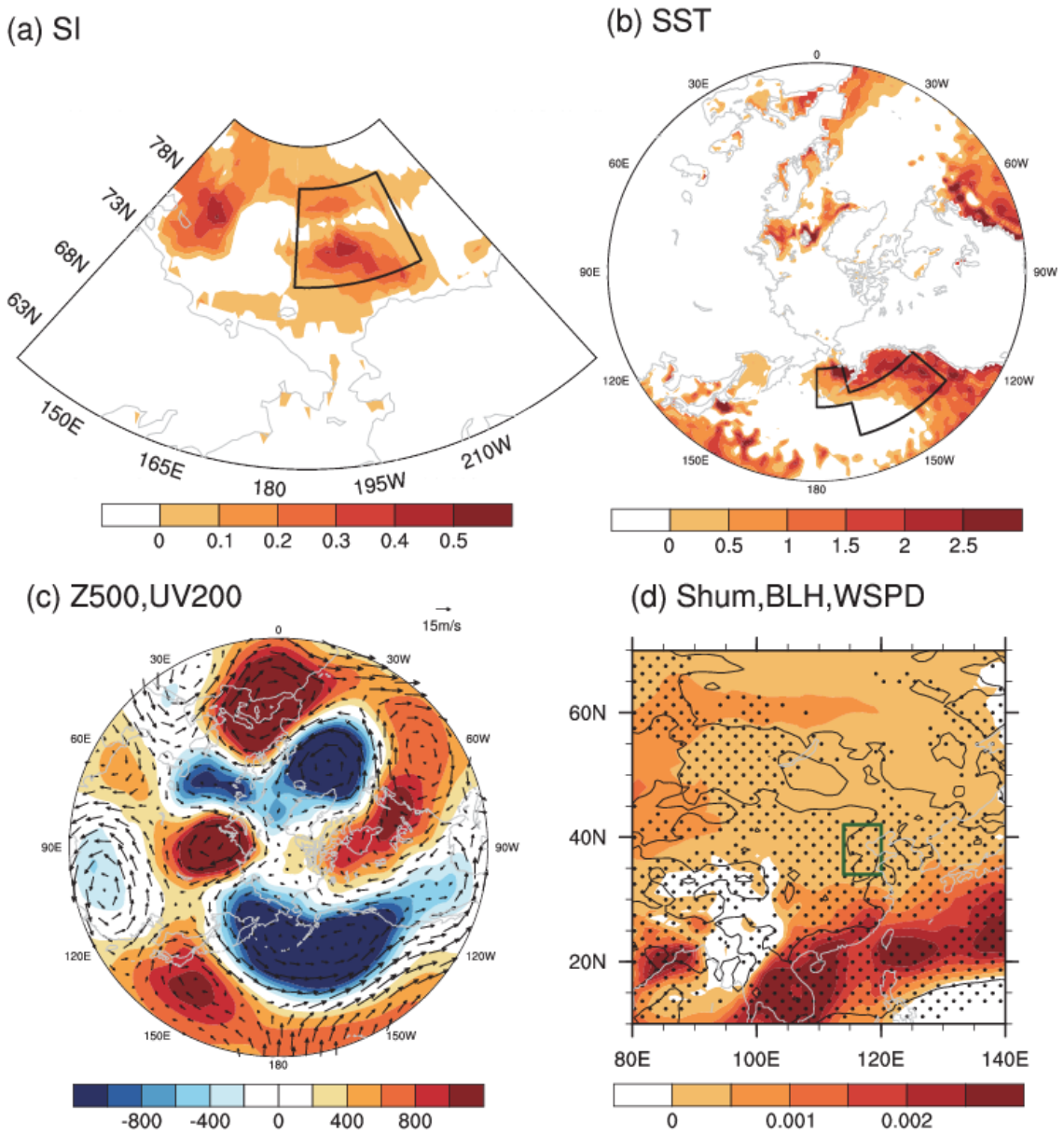

Figure 1~~6~~7. The distributions of (a) September-October sea ice concentration in 2015, (b) sea surface temperature in November 2015, (c) geopotential height (shading) at 500 hPa, wind (arrow) at 200 hPa in December-January 2015, (d) specific humidity (shading) at 1000 hPa, BLH (black dots indicate that its value is negative), WSPD (contour, solid black lines indicate a negative value) in December-January 2015. The black box in panel (a) represents the location of the Beaufort Sea, and in panel (b) it represents the BA area. The linear trend was removed.